

Review

# Natural Materials—Interesting Candidates for Carbon Nanomaterials

Arun Kumar<sup>1,2</sup> <sup>1</sup> Department of Computer Science, University of Verona, 37134 Verona, Italy; arun.kumar@mdm.imm.cnr.it<sup>2</sup> CNR-Institute for Microelectronics and Microsystems, Via C. Olivetti, 2, 20864 Agrate Brianza (MB), Italy

**Abstract:** This review sums up the techniques used for the synthesis of carbon nanotubes (CNTs), carbon nanofibers (CNFs), and carbon nanospheres (CNSs) by employing catalysts of natural origin. Establishing large-scale production and commercial applications of CNTs for a sustainable society is still of high apprehension. In this regard, one of the major factors is the starting materials such as precursors and catalyst sources. However, natural materials contain a minor quantity of metals or metal oxides and could be employed as a catalyst source for the synthesis of CNTs, providing the possibility to replace expensive catalyst sources. A large number of successful studies have been completed so far and confirm that these developed methods for carbon nanomaterials synthesis exhibiting high quality from common natural materials are not only possible but, most importantly, promising and scalable. This review also highlights purification methods and recent promising applications of as-synthesized CNTs.

**Keywords:** carbon nanotubes; carbon nanomaterials; natural materials; mineral catalyst; carbon



**Citation:** Kumar, A. Natural Materials—Interesting Candidates for Carbon Nanomaterials. *Physchem* **2021**, *1*, 4–25. <https://doi.org/10.3390/physchem1010002>

Received: 18 December 2020

Accepted: 11 January 2021

Published: 19 January 2021

**Publisher's Note:** MDPI stays neutral with regard to jurisdictional claims in published maps and institutional affiliations.



**Copyright:** © 2021 by the author. Licensee MDPI, Basel, Switzerland. This article is an open access article distributed under the terms and conditions of the Creative Commons Attribution (CC BY) license (<https://creativecommons.org/licenses/by/4.0/>).

## 1. Introduction

The presence of multi-walled carbon nanotubes (MWCNTs) in Damascus steel was the first observation of CNTs in ancient items dated back to the sixth–eighth centuries [1]. Recent discoveries on the existence of CNTs in ancient items as black coatings on the interior walls of pottery shards mined from Keeladi, Tamilnadu, India, dated back to the sixth–third centuries BC [2]. Moreover, the previous work claimed the sighting of CNTs in the Keeladi shards to be the oldest among the nanostructures reported so far from ancient artifacts around the world. These discoveries confirm our understanding that carbon nanomaterials have been a part of our society for centuries. Meanwhile, in the modern era ever since CNTs were discovered [3], they immediately received the focus of the scientific community. CNTs have provided scientific evidence that they are one of the most fascinating and promising nanomaterials. CNTs, being the most widely investigated nanomaterial, have shown remarkable thermal [4–8], electrical [9–12], and mechanical [13–16] properties and have led to potential applications in electronics [17–22], sensors [23–28], drug delivery [29–31], hydrogen storage [32–34], energy storage [23,24,28,35–40], catalysts [23,39,41,42], and other nanotechnologies' [43–47] performances.

The realization of carbon nanomaterials intended for advanced applications on a large scale will definitively face routine production issues, such as the checks on limited existing resources, the cost of materials such as precursors and catalyst sources, and the amount and cost of energy used in the synthesis. These standard factors will also become the key cost drivers for the final product. Successfully putting them into practice, however, requires that the material can be produced at a large scale at a low price. In this regard, many efforts have been made to find simple technologies for large-scale production of CNTs at low cost [48]. Single-walled carbon nanotubes (SWCNTs), double-walled carbon nanotubes (DWCNTs), and MWCNTs have been productively and controllably synthesized via the catalytic chemical vapor deposition (CCVD or CVD) technique [49,50]. Further, it has been proven that a fluidized CVD reactor under the flux of carbon could result in a favorable

way to attain the production of large-scale CNTs [51,52]. Large-scale CNTs production in a fluidized bed reactor is a multidimensional process, ranging from mild catalyst control to CNT agglomerate formation. The structural and morphological properties and qualities of CNTs can be controlled and modulated by the catalyst [53–56]. Hence, for large-scale CNTs production, the role of the catalyst is one of the major factors, while for this, only expensive transition metals such as Ni, Fe, Pt, V, Mo, Co, Y, and La are being actively used [57–59]. For example, in the case of CNTs in ancient items, the catalyst iron (Fe) might have originated from the soil, and then it could have favored the growth of CNTs upon heating the pottery at high temperatures [2]. Any go-ahead factor that reduced the cost of CNTs on a large scale will help in the CNTs applications for the end-user. Therefore, in this regard, one of the key aspects could be the investigations into the search of new inexpensive and effective catalyst sources suitable for large-scale CNTs production.

Metal and metal oxide particles could be easily available in smaller amounts in almost all natural materials and could be used for CNTs synthesis. The growth of carbon nanomaterials employing natural materials as catalyst sources could be a significant solution towards lessening our current dependence on non-renewable and expensive catalyst sources for large-scale production.

In this review, a spectrum of methods and materials for carbon nanomaterials synthesis directly from natural materials is provided. A range of minerals and mineral oxides of natural origin are described herein. Various techniques and hydrocarbon precursors employed for the synthesis of CNTs, CNFs, and CNSs are discussed. These techniques, which can easily transform common natural materials into products of high-added value, are evaluated in detail. The focus remains on the degree of structural analysis of the obtained nanomaterials. It is dealt with in detail because, from an application perspective, only a material of appropriate quality may give rise to its implementation in high-performance applications. The growth mechanism and purification methods for the obtained carbon nanomaterials are discussed. Finally, the review is concluded with the employed applications of the as-obtained carbon nanomaterials in brief, which should be taken into consideration to spread this sustainable concept for the benefit of society.

## 2. Natural Materials as a Catalyst for Carbon Nanomaterials

### 2.1. Garnet

Garnet is a natural mineral having uniform physio-chemical and microstructural properties. Endo and colleagues employed garnet powder having a particle size around 200  $\mu\text{m}$  (from Ube Sand Kogyo, Japan), as a catalyst source for MWCNTs synthesis [60]. They positioned the oxidized garnet powder in a fixed-bed reactor under the flux of city gas containing methane, ethane, isobutene, n-butane, propane, and dimethyl sulfide as an additive to detect the aid of scent. The produced CNTs had diameters in the range of 20–50 nm and unveiled a structure of high order with large-diameter hollow cores (Figure 1). Synthesized CNTs produced by this group showed a high-order structure, even at a relatively low growth temperature (850 °C). They observed that the air oxidation before the flux flow of hydrocarbon results in enhancing the CNTs growth and yield. They observed that air oxidation of iron oxide ( $\text{Fe}_2\text{O}_3$ ) in the garnet transforms  $\text{Fe}_x\text{O}_y$  to  $\text{Fe}_2\text{O}_3$ . Finally, this  $\text{Fe}_2\text{O}_3$  was reduced under the flux of methane ( $\text{CH}_4$ ) and hydrogen ( $\text{H}_2$ ) to leave active Fe particles on the external sand surface. This was also observed in TEM analysis, see Figure 1c. TEM images also reveal the high degree of graphitization of the CNT walls. Further, a wet chemical process was employed for the separation of CNTs, which is discussed in Section 3.

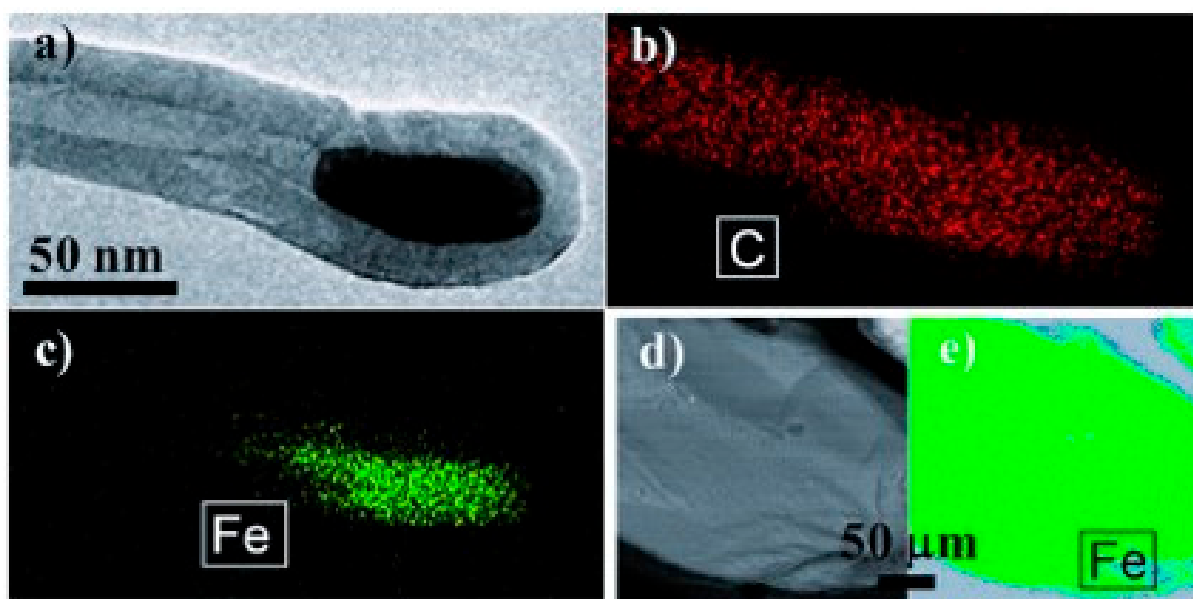


**Figure 1.** (a) TEM image of a carbon nanotube (CNT) tip comprising a catalyst particle. (b,c) EDS elemental mapping showing C and Fe, respectively. (d,e) SEM image and its corresponding Fe mapping image, respectively [60]. Copyright © 2008 WILEY-VCH Verlag GmbH & Co. KGaA, Weinheim. Reprinted with permission from John Wiley & Sons.

## 2.2. Forsterite, Disposide, Quartz, Magnesite, and Brucite

Kawasaki and colleagues confirmed that SWCNTs can be synthesized on magnesite crystals via CH<sub>4</sub> gas pyrolysis [61]. They exploited five natural mineral samples, namely, forsterite, diopside, quartz, magnesite, and brucite, coming from the USA, Pakistan, Japan, Brazil, and the USA, respectively. Despite being a common magnesium silicate, forsterite is an olive group end-member with Mg, while diopside is Ca-Mg pyroxene. Quartz (SiO<sub>2</sub>) is a commonly found natural mineral. Magnesite, a magnesium carbonate (MgCO<sub>3</sub>), and brucite, a magnesium hydroxide (Mg(OH)<sub>2</sub>) mineral, are commonly used for MgO minerals formation. X-ray fluorescence (XRF) measurements on all the samples detected the presence of Fe as a major element in the mineral compositions, while in the cases of magnesite and brucite, the Fe content was about 0.10 and 0.33 wt%, respectively. The mineral samples were first crushed and powdered in an agate mortar and pestle and the obtained powders were employed as a catalyst source for the CVD process under the flux of argon (Ar)-diluted CH<sub>4</sub> gas. After CVD treatment, they observed only a trivial amorphous carbon on the forsterite, diopside, and quartz mineral samples, while, for the magnesite sample, SWCNTs having a 1.0–1.8 nm diameter were obtained. Usually, CNTs are arranged in bundle forms with diameters of the 5–20 nm range along with double-walled CNTs (DWCNTs). SWCNTs were also observed to be grown on natural brucite. Further, it might be anticipated that no CNTs would grow on quartz, due to the lacking Fe content, while it was unexpected that even forsterite and diopside were not able to catalyze the CNTs' growth despite the fact that they contain a high amount of iron. It could be because the Fe content in these minerals is not reachable to the hydrocarbon during the CVD growth process. SWCNTs have a single wall and thus require smaller catalyst particles as compared to MWCNTs, allowing the prediction that the minor Fe content in magnesite and brucite permits the materialization of small Fe catalyst particles which act as a catalyst source for the SWCNTs' growth [61].

## 2.3. Chrysotile

Chrysotile is a low-cost natural material composed of fiber bundles having a lamellar structure of phyllosilicate. Chrysotile's crystalline structure is formed by the interface between layers of tetrahedral tridymite, SiO<sub>4</sub>, and the octahedral layers of brucite, Mg(OH)<sub>2</sub>, having resultant curvature in the structure. However, its surface properties can be altered

through functionalization or coating with materials with specific characteristics. Lemos and colleagues [62] used chrysotile ( $\text{Mg}_3\text{Si}_2\text{O}_5(\text{OH})_4$ ) from mining waste (supplied from Sama Minerações Associadas) impregnated with 20 wt% Co using cobalt(II) nitrate hexahydrate ( $\text{Co}(\text{NO}_3)_2 \cdot 6\text{H}_2\text{O}$ ) for carbon structures' growth using ethanol via CVD at the growth temperature range of 600–900 °C, as represented in Figure 2. The ethanol decomposition can form different carbon nanostructures in the form of CNTs, CNFs, and amorphous carbon, as well as graphitic layers around the catalyst [62]. They detected that following to the CVD process, all materials were found to be coated with a high amount of carbonaceous structures along with silicate fibers, though they were more agglomerated and larger in comparison to the chrysotile before the CVD process due to sintering and phase changes. The highest carbon nanomaterials yield was obtained at the growth temperature of 800 °C. CNT formation on chrysotile was not obtained. Further, they implemented the obtained products for the wastewater treatment, as discussed in Section 4.

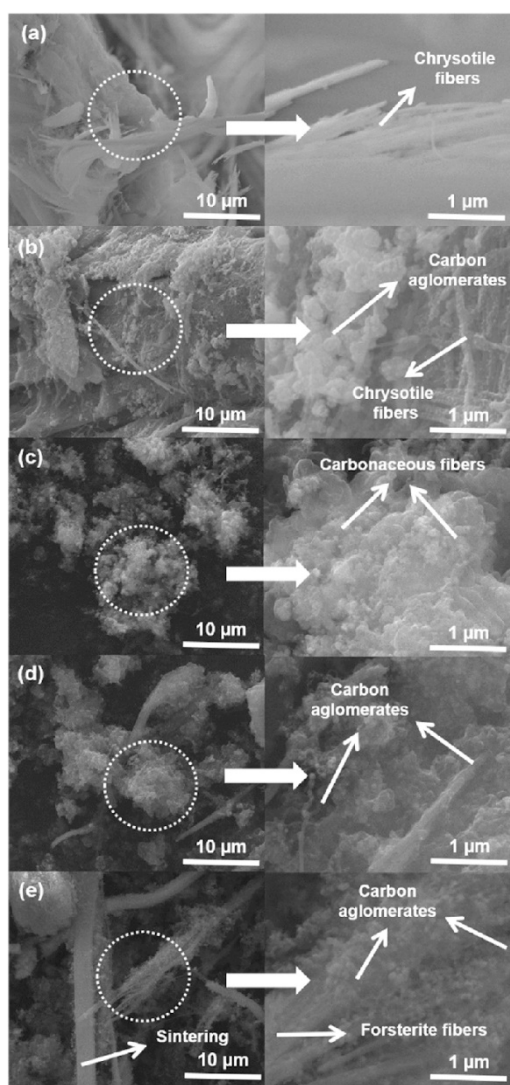


**Figure 2.** SEM images of (a) pure chrysotile, (b) Cris/Co600, (c) Cris/Co70700, (d) Cris/Co800, and (e) Cris/Co900 [62]. Copyright © 2016 Elsevier Ltd. Reprinted with permission from Elsevier.

#### 2.4. Bentonite—Montmorillonite, Zeolite

Bentonite is an absorbent aluminum phyllosilicate, which is generally an adulterated clay typically comprised of montmorillonite. Bakandritsos and colleagues employed natural bentonite having the commercial name Zenith-N from the island of Mylos, Greece, obtained from Silver and Barytine Co. [63]. The raw material was found to contain mont-

morillonite (85%), feldspars (5%), calcite (3%), quartz (2.5%), illite (2%), cristobalite (2%), and the leftover of amorphous matter (0.5%). For CNTs' growth, they placed the materials in a horizontal fixed-bed flow reactor for carbon chemical vapor deposition at 700 °C, using acetylene ( $C_2H_2$ ) diluted with Ar 15% *v/v* gas mixture. The grown carbon nanofibers were found to have a mean diameter of 50 nm.

Further, in 2008, Kadleciková and colleagues used natural montmorillonite (MMT) separated from bentonite from Stará Kremnička, Jelšový Potok, near the quarry at Kremnica, Slovakia [64]. Another sample used was zeolite tuff from the Nižný Hrabovec locality having a particle size of about 10 mm as a 2 mm-thick polished plate. Tuff is a compact igneous rock composed of minerals such as cristobalite, clinoptilolite, feldspars, and quartz. They employed  $CH_4$  in a hot filament CVD reactor for the CNTs' growth. Further, on the quality of the grown CNTs, they studied the effect of catalyst parameters and the  $Fe^{3+}$  cations amount on the surface of the aluminosilicate. The difference that was concluded was that in the event of the particle montmorillonite, they faced a severe problem in the separation of the catalyst from the CNTs phase, while in the case of monolithic zeolite materials, this problem was easy to solve. The optimum mineral catalyst (from the point of view of the amount of CNTs) contains both irons as  $Fe^{3+}$  cations in exchangeable positions and Fe from the solution used to prepare Fe-MMT. They suggested that the main catalytic activity may be attributed to Fe atoms outside the interlayer space of MMT in disparity with Zhang and colleagues' [65] work, where they suggested that the catalytically active particles are Fe atoms in the interlayer space.

Rinaldi and colleagues used bentonite from Winston Company, Germany, sold as Katzenstreu, and cat sand as a support and catalyst source for CNTs' growth, as represented in Figure 3 [66]. The bentonite was at first reduced by hydrogen (75%) in helium. They found that sample was enlarged almost three times when it underwent ethylene flux in the CVD process for 1 hour. MWCNTs with varying wall thicknesses having an outer diameter in the range from 6 to 40 nm were obtained. The complex quality of CNTs could have originated from the various elements' presences, and it was mainly due to the availability of two Fe sources (siderite and armalcolite) in the system. Figure 3d exhibits the HRTEM of the obtained CNTs having a lattice space of 0.21 nm along with the inclusive presence of  $Fe_3C$ . The yield obtained was about 28.7% and the low surface of  $33.1\text{ m}^2\text{ g}^{-1}$  could be due to the loss in microporosity and mesoporosity loss during the reduction process of bentonite. This also led to the fact that the bentonite matrix was not able to rebuild the porous system. The obtained CNTs were found to be of a highly graphitic structural order in comparison to the CNFs obtained on natural lava and soil (discussed in Section 2.8). Further, they tested the mechanical stability of the CNTs/bentonite composite employing the ultrasonic treatment. For this, the obtained sample was immersed into two different types of solutions (water and hexane) and ultrasonication treatment was carried out for 2 h with nitrogen. Later on, they observed that the composite expanded twice the original volume in water solution without any noticeable suspended matter, while in the case of hexane, the composite expanded and filled over the container, which could be due to the hexane affinity towards the hydrophobic surface of CNTs. The solution was found to be stable for up to one week without any particle presence. SEM and nitrogen physisorption measurements did not disclose any major change in the morphological summary and adsorption/desorption, respectively. These results indicate the good mechanical stability of CNTs/bentonites composites.

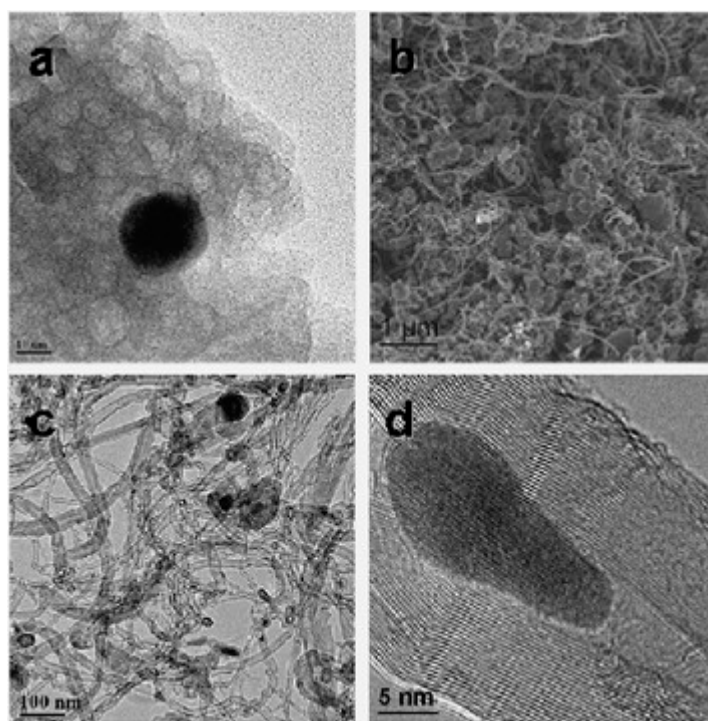


**Figure 3.** SEM and TEM images of bentonite: (a) reduced bentonite, (b) CNTs-bentonite composite, (c) CNT product, and (d) CNT-encapsulated  $\text{Fe}_3\text{C}$  nanoparticle, [66]. Copyright © 2008 The Royal Society of Chemistry 2008. Reprinted with permission from The Royal Society of Chemistry.

In 2018, Huseynov and colleagues used natural bentonite ceramic clays from the Atyali and Gobu deposits of Azerbaijan for MWCNTs' growth [67]. They employed the aerosol chemical vapor deposition technique with two types of carbon sources: cyclohexane—CyH (98%), and n-heptane—Hep (98%). SEM analysis displayed the high-purity and -quality growth of synthesized CNTs without any non-tubular form of carbon (soot, coke, etc.). MWCNTs were fashioned in an extended long filaments shape, having a diameter in the range of 48.2–123.9 nm and being 26.9 mm in length. Further, they employed the MWCNT/natural Azerbaijani bentonite for electro-conductive ceramic composites application, which is discussed in Section 5.

## 2.5. Natural Laterite

Laterite is both a soil and rock type rich in Fe and Al contents and is considered to be formed via intensive and prolonged weathering of the underlying parent rock. Kumar and colleagues employed Ni laterite powder from Tiebaghi in New Caledonia for CNTs and CNSs syntheses via CVD using ethylene as a carbon source [68]. In the used laterite, the major micro-contents found were goethite,  $\text{FeO(OH)}$ , and hematite ( $\text{Fe}_2\text{O}_3$ ) along with a minor amount of phyllosilicates. It was observed that the pristine laterite powder was chemically bound with water, so it was first dehydrated via calcination and then reduced in the following sequence:  $\text{FeO(OH)} > \text{Fe}_2\text{O}_3 > \text{Fe}_3\text{O}_4 > \text{FeO} > \text{Fe}$ , so that it could be effectively subjugated as a catalyst source. They observed that at 700 °C, mainly CNTs grew, while at 800 °C, CNSs started to form. They produced CNTs entangled in a "spaghetti-like" fashion, having a diameter in the range of 10–100 nm, while CNSs had a diameter of 500–700 nm. They clearly observed the existence of metal chunks inside some CNTs, along with amorphous carbon surrounding them, as depicted in Figure 4. Further, they proposed a plausible growth mechanism based on the fragmentation of the pristine iron-containing material, with probable reduction of  $\text{Fe}_2\text{O}_3$  to metallic Fe particles to become the catalysts for CNT growth. They neglected the role of Ni for CNT growth, considering the Ni content to be of a low amount. In the case of CNS growth, they speculated that initially some nanometer-sized catalyst chunks are coated with amorphous carbon, which

in turn prevents the growth of CNTs. Thus, these catalyst chunks, which are now unable to catalyze CNTs, further get coated by amorphous carbon during the remaining growth time.

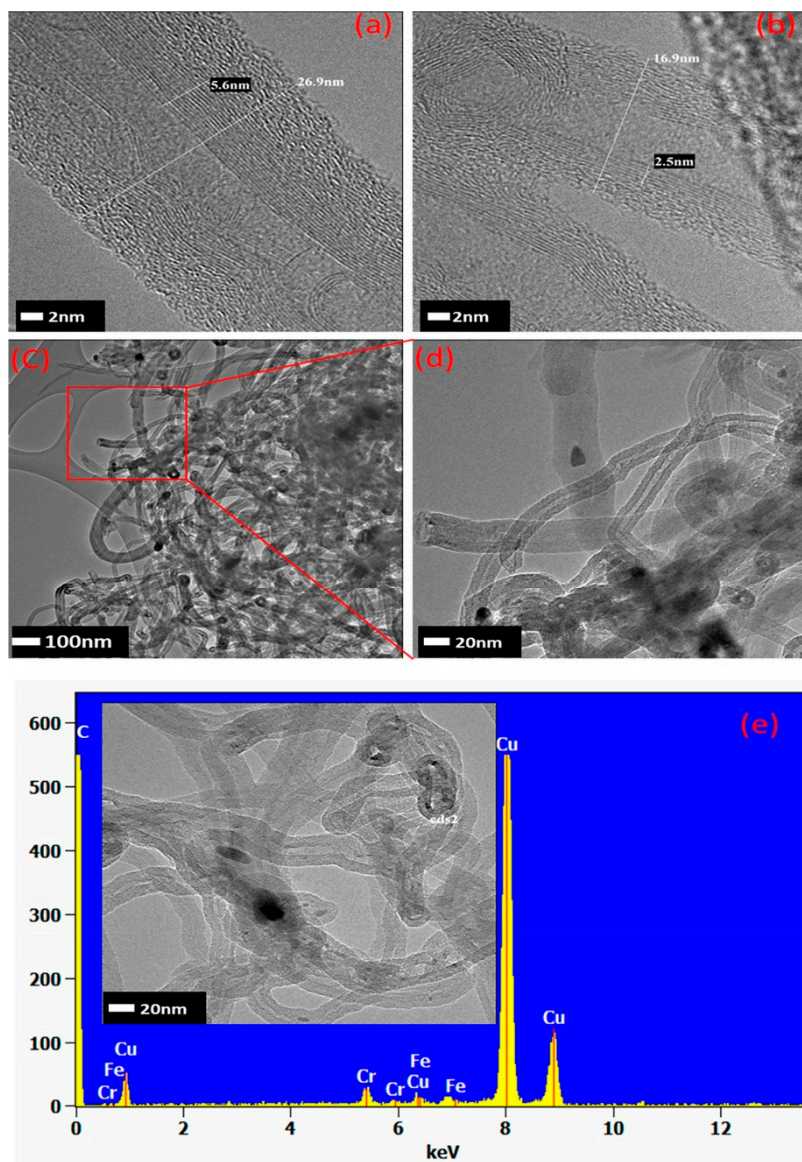


**Figure 4.** (a–d) HRTEM images of the CVD-synthesized CNTs at 700 °C and (e) their EDS analysis [68]. Copyright © 2018 American Chemical Society. Reprinted with permission from American Chemical Society.

#### 2.6. Siliceous Breccia

Siliceous breccia is a natural rock mainly composed of  $\alpha$ -quartz ( $\text{SiO}_2$ ) along with some inclusions of hematite ( $\alpha\text{-Fe}_2\text{O}_3$ ) and goethite ( $\text{FeO(OH)}$ ) [69,70]. Kumar and colleagues used drill core siliceous breccia extracted from a mine in New Caledonia [71], as a catalyst source for the CNT growth via CVD. The effect of the  $\text{H}_2$  addition in the  $\text{C}_2\text{H}_4$  precursor flow was also studied. The weight percent of iron (Fe) measured via EDS was observed to be very low, 0.39 wt.%. Iron was observed with a sub-micrometric presence irregularly dispersed all over the silicate segments, which acts as a catalyst and makes this material a suitable candidate for CNT growth, see Figure 5. The obtained CNTs were arranged in bundle formations having a diameter in the range of 25–35 nm. Moreover, the diluted  $\text{C}_2\text{H}_4/\text{H}_2$  stream changes the ratio of carbon to  $\text{H}_2$  and affects the carbon nanostructures' growth, which results in the growth of CNTs with enhanced length and diameter. CNTs were found all over the catalyst source surface, having some regions containing dense

agglomerations of as-grown CNTs, while some areas over the catalyst source surface did not show any presence of CNTs. This inhomogeneous growth may be because of the non-uniform distribution of iron oxide-hydroxide ( $\alpha\text{-Fe}_2\text{O}_3$ ,  $\text{FeO(OH)}$ ) particles on the siliceous breccia surface.

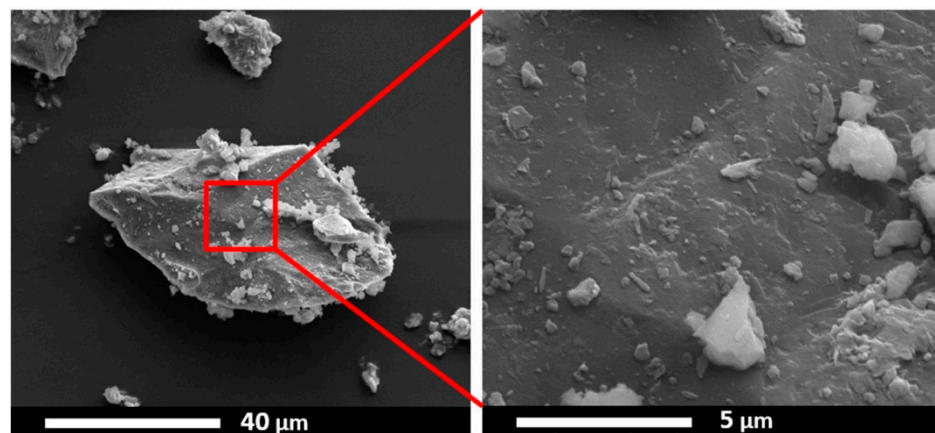


**Figure 5.** ESEM image of the siliceous breccia powder [71]. Copyright © 2019 Elsevier B.V. Reprinted with permission from Elsevier.

### 2.7. Vermiculite

Vermiculite clays are weathered mica having  $\text{K}^+$  in between the molecular sheets and are exchanged by  $\text{Mg}^{2+}$  and  $\text{Fe}^{2+}$  cations during weathering. Zhang and colleagues used vermiculite as a carrier of a catalyst mined from Lingshou, Hebei Province of China [72]. The vermiculite was composed of the following elements:  $\text{SiO}_2$  (42%),  $\text{Al}_2\text{O}_3$  (12%),  $\text{MgO}$  (28%),  $\text{Fe}_2\text{O}_3$  (13%),  $\text{K}_2\text{O}$  (4.0%),  $\text{CaO}$  (0.5%), and  $\text{H}_2\text{O}$  (0.5%), having a particle size of 10–100  $\mu\text{m}$ . Vertically aligned CNTs in large amounts were grown in a fluidized bed reactor using ethylene as a carbon precursor. CNT arrays having a relatively uniform length, an inner diameter in the range of 3–6 nm—while an outer diameter of 7–12 nm—and up to several tens of microns in length were obtained, as shown in Figure 6. The as-grown CNTs possessed good alignment and exhibited a purity of ca. 84%. The results also support the use of a fluidic bed in comparison to a fixed-bed reactor, as the reactor provides a large, effective surface area and plenty of space for CNT growth [73]. Good heat and mass flow ensure the uniform temperature and reactant concentration in the entire fluidized bed, which is one of the key parameters for the controlled growth of CNT arrays.

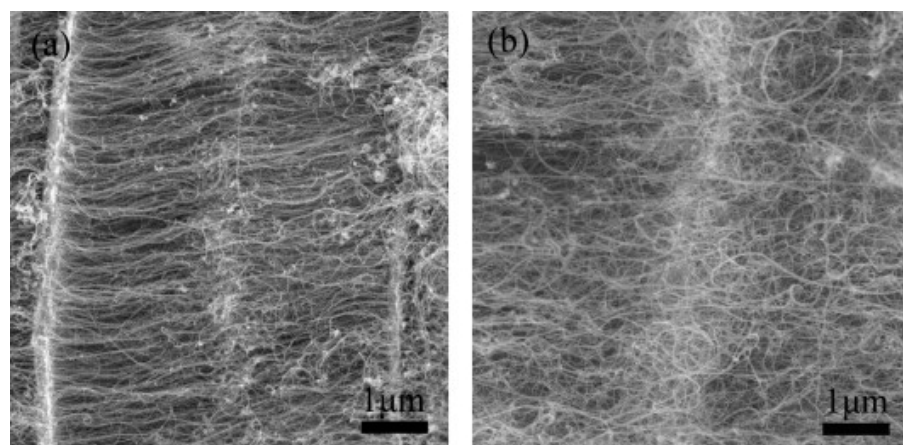


**Figure 6.** SEM images of junctions during CNT array growth time: (a) 15 min and (b) 60 min [72]. Copyright © 2009 Elsevier Ltd. Reprinted with permission from Elsevier.

### 2.8. Natural Lava

Mount Etna lava, a natural material, was employed as a catalyst and support for the synthesis of carbon nanomaterials [74]. Natural lava was first crushed in a powder and later the crushed powder was put into a horizontal quartz reactor and reduced with H<sub>2</sub> before CVD treatment. For the CVD growth at 700 °C, ethylene was employed as a carbon precursor. A mixture of CNTs and CNFs was obtained on the lava rock. The SEM revealed that the obtained carbon nanomaterials were leading in CNF agglomerates. TEM measurements on the obtained CNFs and CNTs showed that they have a graphitic wall structure instead of a normal nanotube or nanofiber. The obtained CNTs and CNFs had a diameter on the scale of nanometers to micrometers. In later works, they were able to synthesize the CNTs/CNFs having excellent thermal stability up to 550 °C in a static air environment [75]. They had been competent enough to reveal that by choosing suitable experimental conditions, the morphology and structure quality of the carbon nanomaterials could be controlled and enhanced. Further, they stated, on the effect of the hydrocarbon flux flow, that upon high flux, the morphology of the carbon nanomaterial is disordered and more graphitic-like structures are obtained, while a lower hydrocarbon flux leads to ordered and well-defined growth of CNTs. Similarly, when the H<sub>2</sub> flux flow was decreased, a significant change in the morphology and order of the carbon nanomaterials (CNFs to MWCNTs) was noticed. Next, upon decreasing the temperature, no significant alteration in the morphology of the carbon nanomaterials was observed.

### 2.9. Blended Iron Formation (BIF)

BIF primarily consists of hematite and magnetite grains alternating to quartz grain bands from thin bands of sedimentary rocks [76]. Luis and colleagues used BIF powder obtained from the Bundelkhand Craton, Northern India, as a catalyst source for the production of N-MWCNTs via aerosol-assisted catalytic chemical vapor deposition (AAC-CVD) [77]. The growth process is represented in Figure 7. Yield production as high as 340% wt./wt. was obtained by 1-hour ball-milled BIF powders, and this indicated that BIF powders can be employed for large-scale CNTs production. The produced CNTs had a diameter in the range of 20–200 nm. N-MWCNTs having diameter of 200 nm were found to have wrinkled or corrugated surfaces. Helical structures with diverse surface morphologies and diameters could be obtained, which could be due to the unevenly shaped catalytic particles. They discussed a possible scenario to explain N-MWCNT morphologies for the high CNT yield. Upon reduction, the Fe<sub>2</sub>O<sub>3</sub> structure embedded inside the BIF nanoparticles is transformed into the α-Fe phase. In their system, small nanoparticles of the catalyst were found to have strong interaction with the SiO<sub>2</sub> substrate, which remain fixed at their respective positions, and this hindered their catalytic performance. Further, this affects the growth of carbon nanomaterials, resulting in the complex NMWCNTs morphology. However, they predicted that the fixed nanoparticles in the system could lead to the thinner MWCNTs with individual longitudinal clumps, separated by the different size of the fixed catalytic nanoparticle. The thick NMWCNTs' growth could be catalyzed by the combination of Fe<sub>3</sub>C and fixed catalytic nanoparticles inside the system. Due to the complexity of the catalytic materials, they tried to explain this phenomenon with several possible conditions (see Figure 8). However, they pointed out that these circumstances must be more thoroughly studied to understand this phenomenon. Further, they proposed the following hypothetical explanation for the high CNT yield obtained. They speculated that, first, the nitrogen coming from benzylamine decomposes at 950 °C and converts into benzyl and amino. They synthesized their samples at 850 °C and it is quite probable that at this temperature, benzylamine is not completely decomposed, resulting in only the interaction of benzyl with the nanocatalyst, leaving a fraction of amino. Minor Fe nanoparticles formed when the BIF sample underwent a reduction for 30 min. The superficial O<sub>2</sub> bond at the SiO<sub>2</sub> nanomaterial was weakened, and the O<sub>2</sub> avoided the negative effect of H<sub>2</sub> from benzyl, supporting the CNTs' growth. They conceptualized that the CNTs yield could be enhanced by controlling the hydrogen activity with the oxygen from the

$\text{SiO}_2$  nanoparticle. In the scenario of  $\text{N}_2$ , MWCNTs yield is decreased due to toluene. The obtained results exhibit that benzylamine increases the CeN which improves the yield of NMWCNTs. Next, they extended their activities to study the electrochemical response of NMWCNTs-composed electrodes in order to examine the obtained nanomaterial for energy storage and sensing applications (see Section 4).

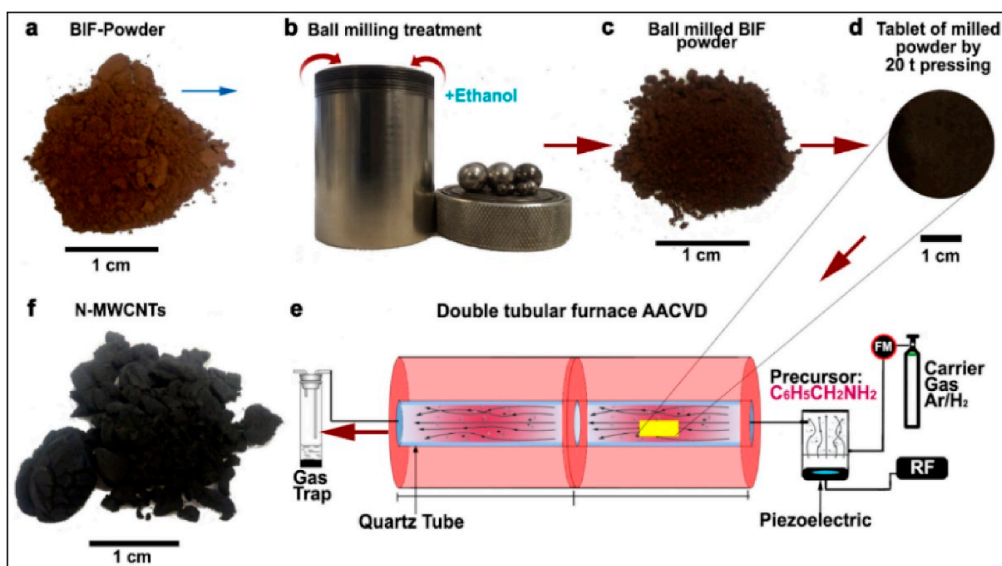


**Figure 7.** Schematic representation of the steps followed to obtain nitrogen-doped multi-walled carbon nanotubes (N-MWCNTs) using the banded iron formation (BIF) material as a catalyst. (a) Initial BIF powder with red-brown color, (b) Ball milling of 5 g BIF powder with 10 mL of ethanol was performed for 1 h, 2 h, and 3 h, (c) the obtained ball-milled BIF powders with dark brown color, (d) the tablet of the milled BIF powder by 20 t pressing, (e) AACVD reactor wherein the tablets were positioned for growth, and (f) the as-obtained N-MWCNTs after growth [77]. Copyright © 2020 Elsevier B.V. Reprinted with permission from Elsevier.

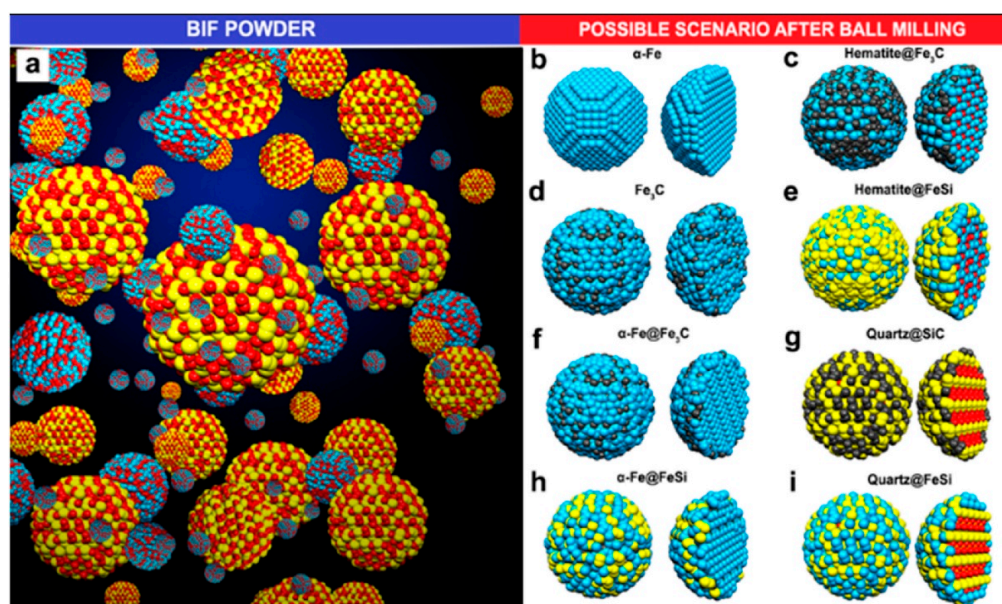


**Figure 8.** Schematic of the proposed scenarios for N-MWCNTs' growth. (a) BIF powder grain's ball-and-stick model and (b–i) possible circumstances after ball-milling process. Blue, red, yellow and black colours represents Fe, O, Si, and C ball-and-stick atoms, respectively. The BIF powder was mainly composed of hematite ( $\text{Fe}_2\text{O}_3$ ) and quartz ( $\text{SiO}_2$ ) particles [77]. Copyright © 2020 Elsevier B.V. Reprinted with permission from Elsevier.

### 2.10. Wollastonite

Wollastonite is a type of calcium inosilicate ( $\text{CaSiO}_3$ ) material and is generally available from commercial mines in the PR of China, the USA, India, Finland, former Yugoslavia, Mexico, Greece, and other countries. Wollastonite shows many useful properties, such as low content of volatiles, high brightness, and whiteness, as well as low absorption of moisture and oil. These characteristics of the wollastonite material pave the way for extensive applications such as ceramic composites, paper, paint, vinyl tile manufacture, and plastics. Zhao and colleagues used wollastonite mined from Jiangxi, PR of China, exhibiting a fibrous structure in the form of needle-shaped crystals, as a natural substrate for the facile synthesis of aligned CNTs [78]. They showed that aligned CNTs could be easily obtained on wollastonite fibrous natural material via CVD. The obtained CNTs revealed good alignment and outer diameters ranging from 4 to 30 nm—while the distribution of the inner diameters ranged from 4 to 12 nm—and length distributions up to 15  $\mu\text{m}$ . Raman spectroscopy evaluations gave values of  $I_D/I_G = 0.54$  (D and G band intensity ratio in the Raman spectrum) for the CNTs, revealing the high degree of crystallization of the CNTs. Thermogravimetric analysis (TGA) in air showed that about 30 wt% of the wollastonite/CNT hybrid corresponded to CNTs with a sharp and narrow derivative thermogravimetric (DTG) peak with a high ignition temperature ( $676.1^\circ\text{C}$ ), indicating the high quality of CNTs, see Figure 9. Further, the as-grown CNT arrays were easily purified to ca. 98.7%, providing a scalable route towards high-value, advanced materials with extraordinary performance.

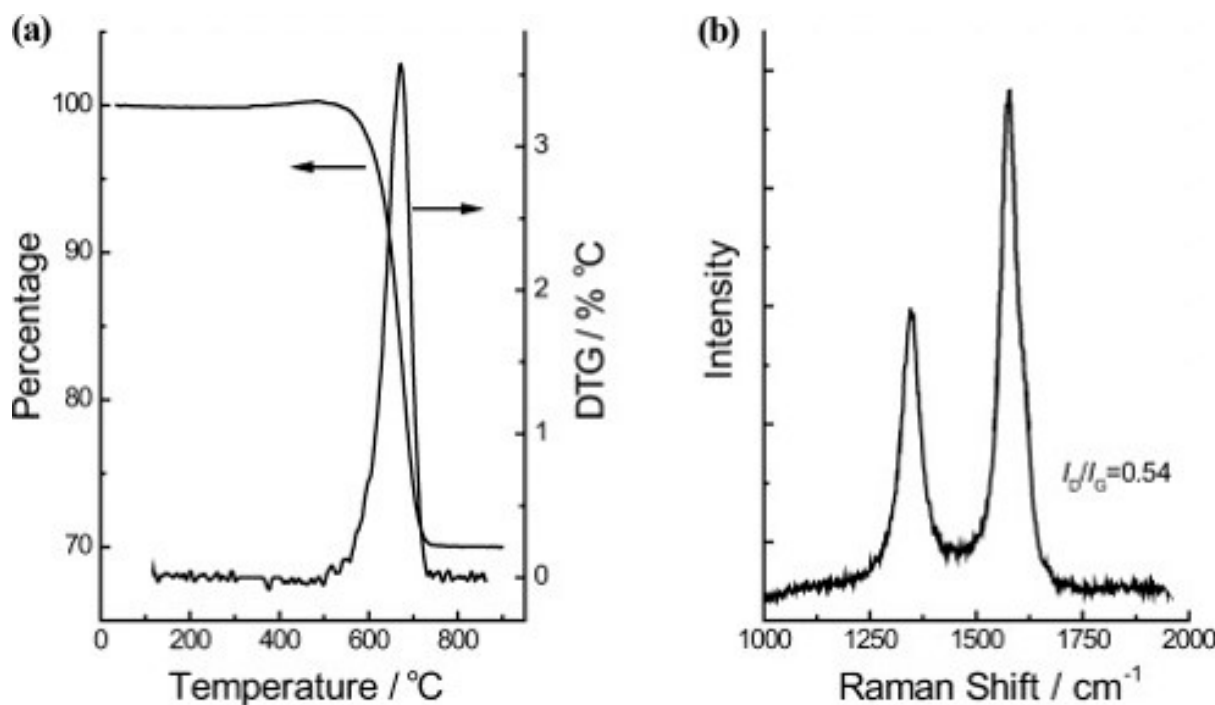


**Figure 9.** (a) TGA and DTG curves, and (b) Raman spectrum of the wollastonite/CNT hybrids yield [78]. Copyright © 2010 WILEY-VCH Verlag GmbH & Co. KGaA, Weinheim. Reprinted with permission from John Wiley & Sons.

### 2.11. Kaolinite, Nontronite, and Sepiolite

Sepiolite is a naturally occurring soft clay, with microcrystalline-hydrated magnesium silicate of the chemical formula  $\text{Mg}_4\text{Si}_6\text{O}_{15}(\text{OH})_2 \cdot 6\text{H}_2\text{O}$ . Sepiolite has a low specific gravity, microfibrous morphology, and high porosity. Nie and colleagues employed sepiolite as a catalyst source mined from Nanyang, Henan Province of China [79]. They used sepiolite as the catalyst without any pre-treatment in a fixed-bed reactor with  $\text{CH}_4$  as a hydrocarbon source. After growth, small bundles of SWCNTs entangled with each other with a length

of several hundred microns. SEM images showed a single graphene layer with minute defects. Further, they showed that more than 90% of the obtained products were SWCNTs. The size of the Fe catalyst cluster observed was about 20 nm. The diameters of the obtained SWCNTs ranged from 1 to 40 nm depending upon temperature and the amount of metal loading. The chirality and diameter distribution were highly dependent on the reaction temperature. Raman spectroscopy was employed to analyze the graphitization degree and the diameter distribution of the obtained SWCNTs. Raman intensity ratios of the D to G bands were 0.07, 0.14, and 0.08 under the excitation wavelength of 633, 514, and 532 nm, respectively (Figure 10a–c). This indicates the high degree of graphitization for the as-grown SWCNTs. On the other hand, sharp RBM peaks were also observed in different Raman spectra. The diameter distribution of obtained SWCNTs products was estimated by the following equation:  $x = 248/d$  [80]. The strong peaks appeared on the RBM patterns at all the excitation wavelengths, namely, 633, 514, and 532 nm, with the corresponding diameters in the ranges of 1.0–1.9, 1.3–1.8, and 0.8–1.9 nm, respectively. The CNT obtained via this method was further employed for phenol absorption, which is discussed in Section 4.

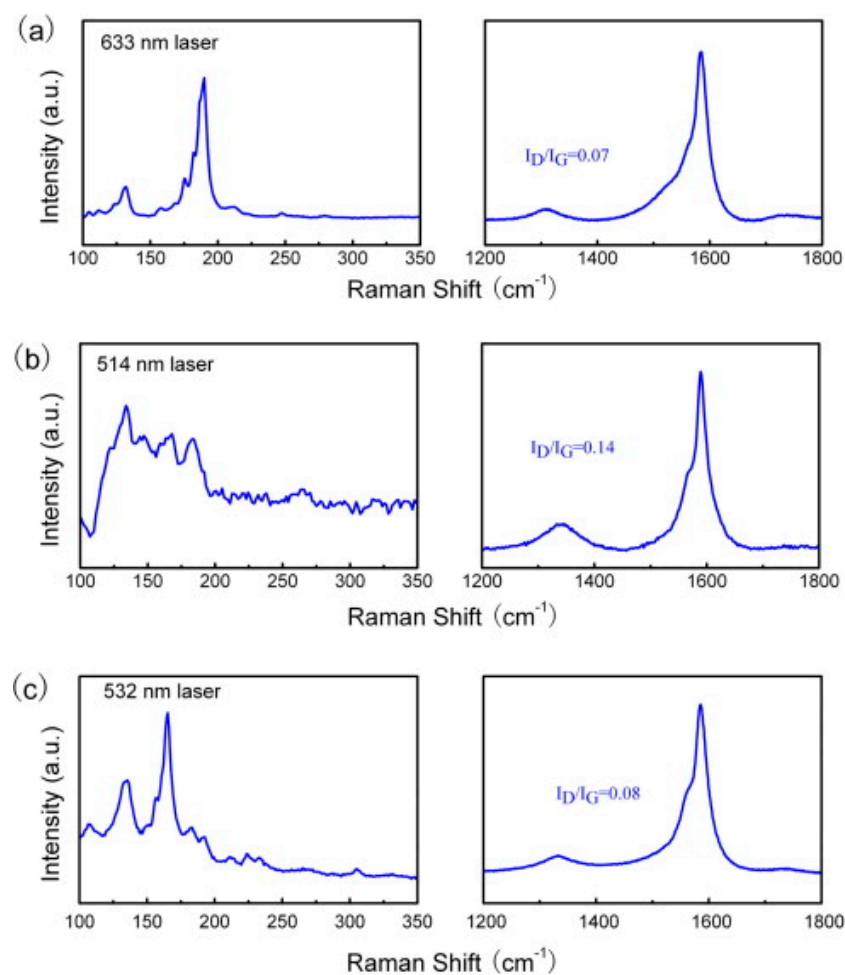


**Figure 10.** Raman spectra of the single-walled carbon nanotube (SWCNT) at the different excitation wavelengths: (a) 633, (b) 514, and (c) 532 nm [79]. Copyright © 2010 Elsevier Ltd. Reprinted with permission from Elsevier.

Additionally, kaolinite, nontronite, and sepiolite are the types of microcrystalline phyllosilicates. Astorková and colleagues used kaolinite (commercial name kGa-2), clay from Warren County, Georgia, USA, nontronite (NAu-2), natural dark-brown clay from Uley Mine, South Australia, and sepiolite (SepSp-1) from Valdemore, Spain, as catalyst sources for CNTs synthesis via hot filament chemical vapor deposition (HFCVD) [81]. As

nontronite belongs to clay minerals with a high Fe content, this material was not modified, while kaolinite and sepiolite were doped with catalytically active metal particles. The diameter distribution of MWCNTs grown on nontronite ranges from 10 to 50 nm with different shapes, see Figure 11a. For example, chain-like nanotubes are made of hollow carbon cages that are interconnected so that the open end of one cage is joined with the dome of another one. In Figure 11b, we can see the bamboo-shaped CNTs. EDS on CNT/nontronite identifies the presence of iron but also Al and Ca, indicating that the Fe particles help in the growth of CNTs. Further, it was found that, in the case of kaolinite, the nanotubes are located between single crystallites; they grow through the whole volume and create 3D grids. In the cases of nontronite and sepiolite, the CNTs grow through the volume of the mineral while creating an additional identifiable discrete phase. While it was observed that CNTs are non-aligned on nontronite, they are aligned in the case of sepiolite.

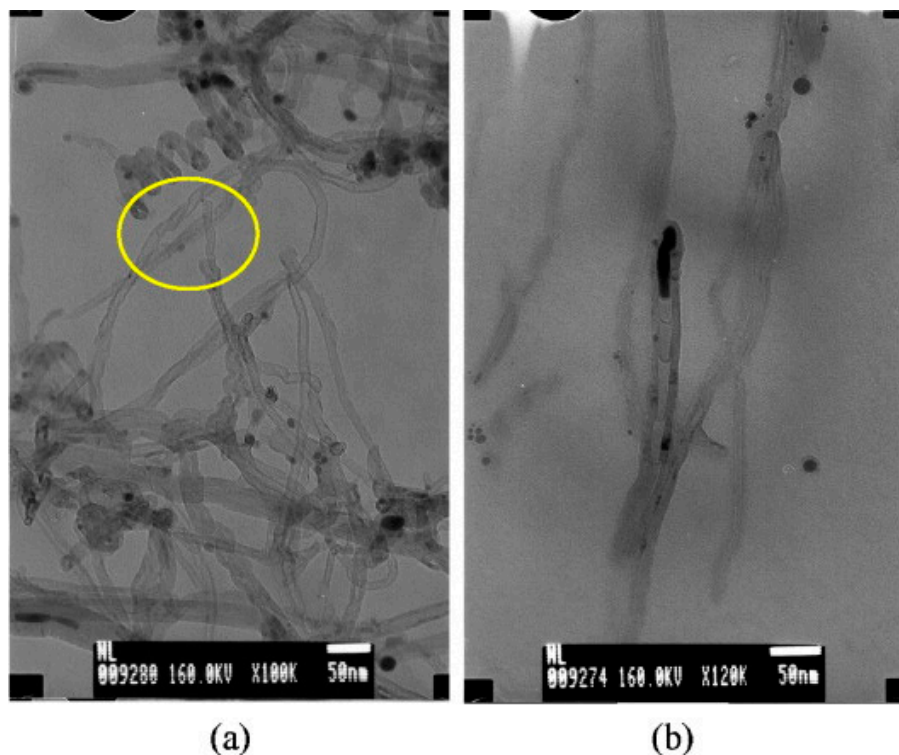


**Figure 11.** (a) TEM image of the carbon grown on nontronite. (b) TEM micrograph of a bamboo-like structure of CNTs [81]. Copyright © 2011 Elsevier B.V. Reprinted with permission Elsevier.

### 3. Purification: The Bridge between Synthesized CNTs and Applications

The mass-produced CNTs from natural materials inevitably contain impurities, mainly in the form of trace elemental particles and carbonaceous impurities (e.g., amorphous carbon and carbon nanoparticles). The impurities present inside as-synthesized carbon nanomaterials limit the full understanding of the growth mechanism, properties, and their applications on a larger scale. Thus, extremely effective and efficient purification methods for the separation of CNTs from the natural complex system is of utmost importance. For CNTs, purification through various general methods such as wet chemical and physical treatment is being conducted.

Endo and colleagues employed a wet chemical process for the separation of CNTs grown on garnet sand, by simply using an ultrasonic bath in a water suspension [60] (see Figure 12). The simplicity of a separation process such as this is important due to the exclusion of strong acids being used for removal. On the other hand, such a wet chemical treatment can introduce defects in CNTs and change their surface chemistry by functionalization.

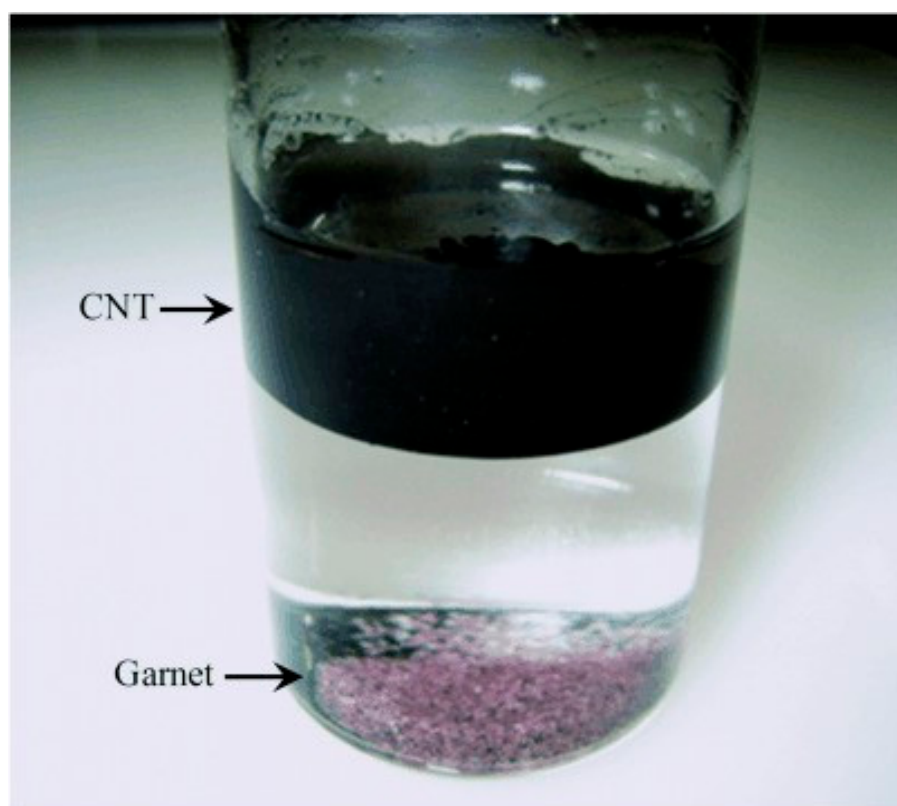


**Figure 12.** Photograph showing CNTs and garnet sand particles separation [60]. Copyright © 2008 WILEY-VCH Verlag GmbH & Co. KGaA, Weinheim. Reprinted with permission from John Wiley & Sons.

Zhang and colleagues [72] used acid treatment for the purification of CNTs, where they showed that vermiculite present inside the CNTs could be removed by dispersing the obtained carbon nanomaterials in the 3.0 mol/L HCl solution for one hour and later in the 1.0 mol/L HCl solution. Figure 13a depicts a large vessel full of vertically aligned CNTs grown on an Fe/Mo/vermiculite catalyst. Figure 13b exhibits the SEM image of CNTs obtained after the acid treatment purification, without the presence of vermiculite layers. They explained that the obtained CNTs were found to have good alignment. However, the CNTs seemed to be disordered and in contrast to the claimed vertically aligned CNTs in Figure 13a, labeled on a large vessel. Moreover, the CNTs purity was found to be increased from 84.0% to 97.5%.

Further, for the purification of CNTs from natural materials, mainly the use of an acid and an alkaline is conducted to react with the metal catalyst/support present inside the CNTs. [63]. The details of these purification methods have been well studied and documented. The pure carbon phase was gained after dispersing the clay matrix substrate with an aqueous mixture of acids comprising of 12% HF and 12% HCl, without any catalyst presence [63]. For obtaining the aligned CNTs with a low diameter and purification up to 98.7%, researchers carried out HF treatment [78], see Figure 14. CNTs produced on a large scale have issues with strong entanglements and impurities, so in this regard, developing efficient and effective routes for CNTs application requires further optimization and additional results on purification methods.

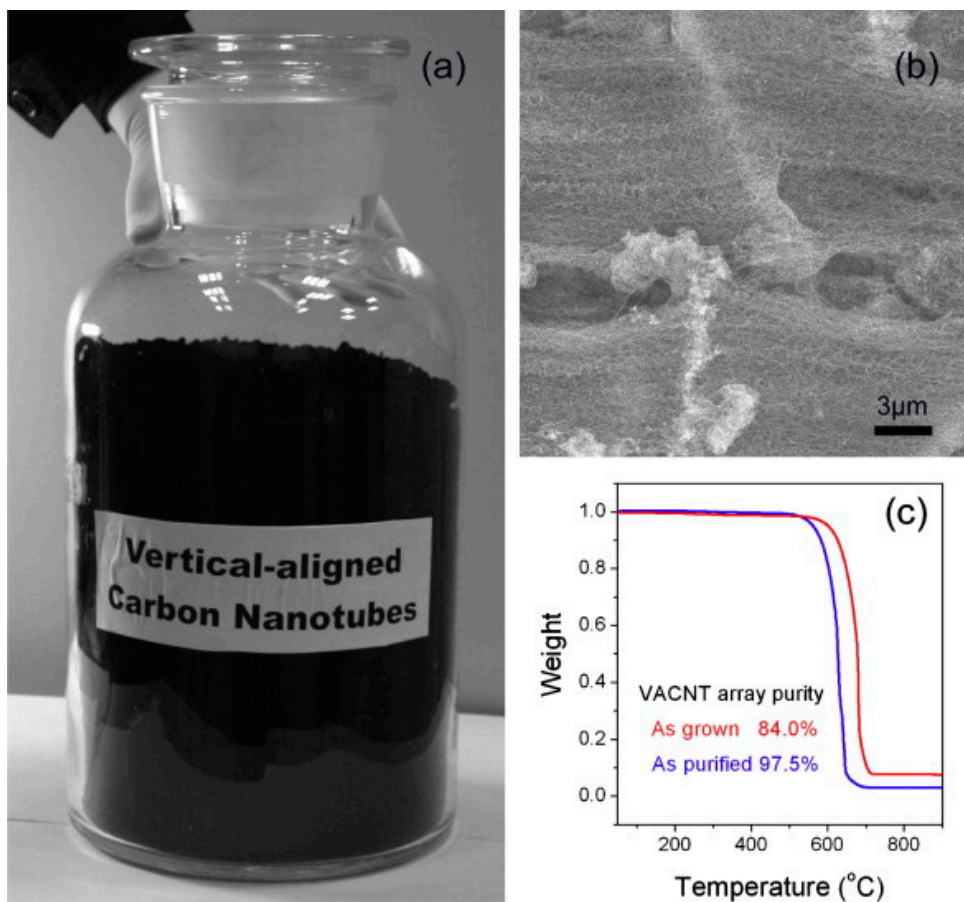


**Figure 13.** (a) A large amount of CNT arrays grown on an Fe/Mo/vermiculite catalyst, (b) SEM image of the as-purified CNTs, and (c) TGA curves of the as-grown and -purified CNT array [72]. Copyright © 2009 Elsevier Ltd. Reprinted with permission from Elsevier.

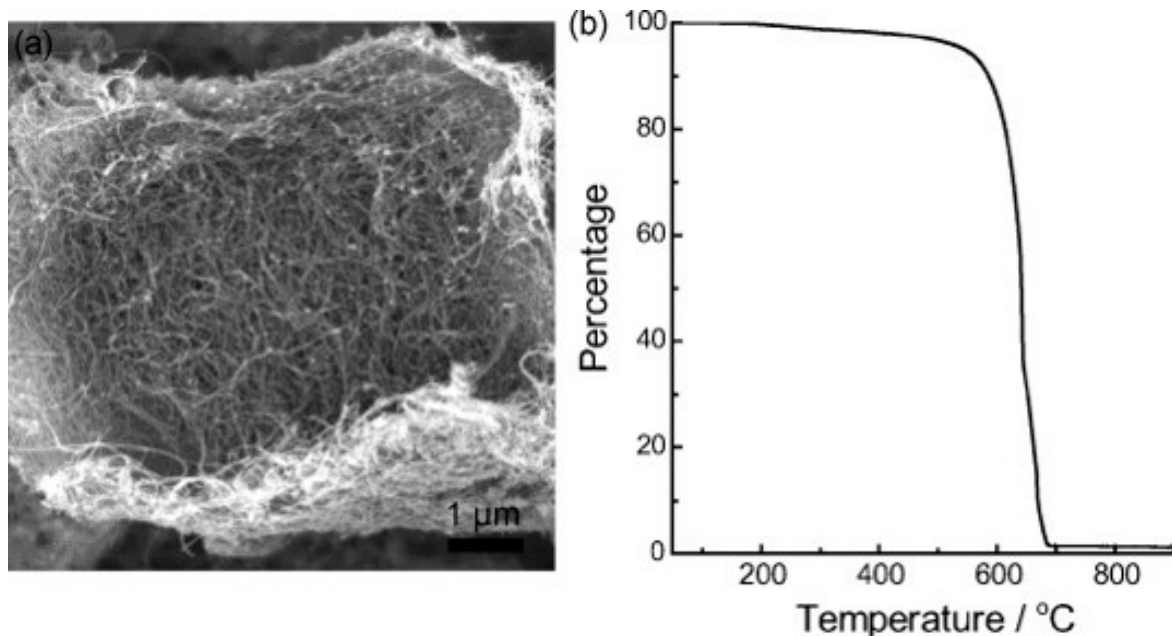


**Figure 14.** (a) SEM image and (b) TGA curve of the purified aligned CNTs after hot filament (HF) treatment [78]. Copyright © 2010 WILEY-VCH Verlag GmbH & Co. KGaA, Weinheim. Reprinted with permission from John Wiley & Sons.

#### 4. Application of the Carbon Nanomaterials Produced through Natural Materials

CNTs are being widely explored for applications in various fields. Significant work has been carried out on potential applications in the area of nanocomposites and energy storage, while the exploration of carbon nanomaterials synthesized using natural materials has not occurred on a large scale from the application point of view. However, scientists have started exploring these materials. In this section, brief citations of some composites and their applications are summarized, which could be employed for large-scale applications.

Water quality has been decreasing exponentially due to an increase in industrialization and extensive human activities leading to large-scale water pollution by discharging the untreated waste directly into the natural environment [82]. In this regard, phenol and phenolic compounds, due to their high toxicity at low concentrations, have been classified as highly carcinogenic and pollutant [83]. Removal of phenol from aqueous solutions has been an important challenge faced by researchers and many efforts have been made in this direction. However, for water and wastewater treatment, activated carbon has been one of the common adsorbents [84,85]. Nie and colleagues investigated the performance of SWCNTs/cal-sepiolite in the adsorption of phenol [79]. The excellent phenol adsorption ability of SWCNTs/cal-sepiolite can be explained by the phenomenon that the presence of the p-electron region on the SWCNTs' (p-electron donors) surface interacts with the phenol adsorption (p-electron acceptor), resulting in a p-p electron donor–acceptor. The as-synthesized SWCNTs/calcined-sepiolite showed excellent ability in phenol adsorption, with an adsorption capacity of 155.8 mg/g, which was considerably more than that on natural sepiolite (12.7 mg/g), see Figure 15 (the hollow symbols are experimental data and the solid lines are the Langmuir model). The obtained results encourage researchers to employ natural materials in advanced materials for environmental applications on a large scale.

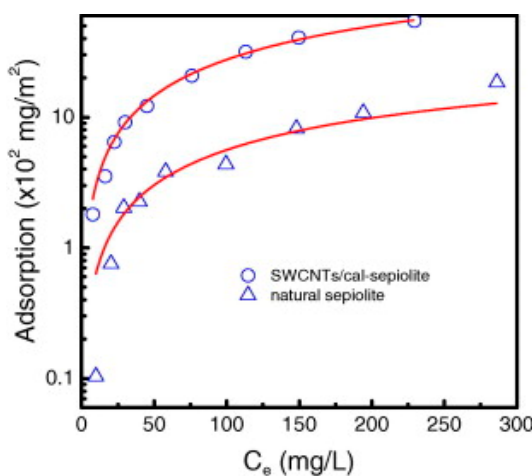


**Figure 15.** Adsorption isotherm of phenol on SWCNTs/cal-sepiolite and natural sepiolite at 30 °C [79]. Copyright © 2010 Elsevier Ltd. Reprinted with permission from Elsevier.

Further, organic components from the textile industry contribute severely to water pollution. In this regard, the effluent color is one of the major appearing indicators [86]. The use of synthetic dyes in major industrial processes is a threat to the ecosystem [87]. The discharge of colored synthetic dyes such as methylene blue (MB) dye is visually invasive and can cause a water body by hindering light penetration as well as oxygen dissipation [88,89]. Therefore, to resolve this problem, researchers have considered carbon materials as an adsorbent to remove the organic and inorganic contaminants from the water [86]. Lemos and colleagues used chrysotile-CNT (discussed in Section 2.3) composites for turbidity removal from biodiesel wastewater and in methylene blue (MB) solutions discoloration by using a heterogeneous Fenton-like process [62]. Figure 16a shows the removal of turbidity using the materials obtained after the CVD process. They obtained

chrysotile-CNT at various growth temperatures (Cris/Co 600–900 °C). Cris/Co800 showed the best removal efficiency in terms of turbidity for all reuse tests. After the adsorption process, the material dispersed in the emulsion was magnetically removed, resulting in the turbidity removal of the system. Further, the magnetic materials were also tested for the subtraction of organic impurities from the aqueous solutions by adsorption followed by oxidation via a heterogeneous Fenton process using the cationic dye methylene blue (MB) as a substrate (Figure 16b). The highest color removal efficiency was achieved for the Cris/Co800 (87%) sample. Surface charges determined by zeta potential experiments were  $-15.01$ ,  $-15.70$ ,  $-17.87$ , and  $-15.37$  mV for Cris/Co600, Cris/Co700, Cris/Co800, and Cris/Co900, respectively, suggesting that the surface of composites shows affinity and should have a good interaction with positively charged molecules, such as MB molecules. Low MB adsorption of pure chrysotile in aqueous media can be understood as a zeta potential value with a surface charge of  $+7.36$  mV. Conversely, upon heating the chrysotile at 900 °C, it transformed to forsterite, resulting in a negative surface charge,  $-14.67$  mV. After the addition of hydrogen peroxide,  $H_2O_2$ , there was a great color removal of the MB solution, which is related to oxidative degradation of the dye molecules.

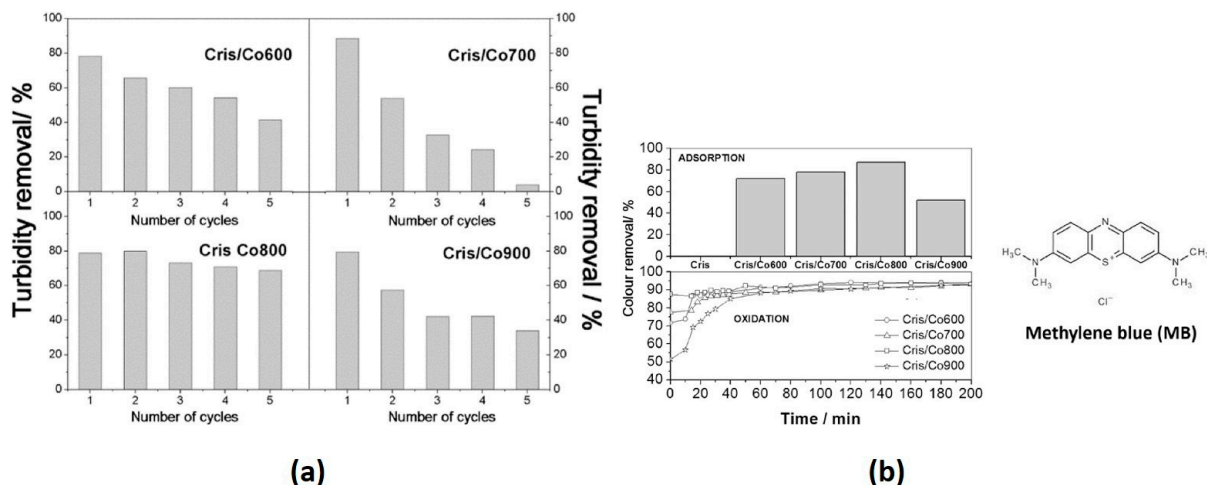


**Figure 16.** (a) Turbidity removal of a real effluent sample from biodiesel production promoted by different composites and (b) discoloration of MB by adsorption after 24 h contact (above), followed by oxidation with  $H_2O_2$  (below) [62]. Copyright © 2016 Elsevier Ltd. Reprinted with permission from Elsevier.

Ceramics reinforced with carbon nanomaterials have shown significant improvements in the areas of mechanical properties, high thermal stability, and high conductivity [90–93]. Huseynov and colleagues employed MWCNTS as electro-conductive ceramic composites [67]. Moreover, it was found that the incorporation of MWCNTs into the ceramic matrices can lead to a remarkable increment in electro-conductivity of MWCNT/bentonite ceramic composites, and the maximum value of electro-conductivity was found to be 8 wt% of MWCNTs. They were able to demonstrate that by increasing the mass fraction of MWCNTs from 1% to 8% in MWCNTs/bentonite ceramic composites, the electrical conductivity enhances substantially. The improvement in electrical conductivity of the composites explained the mass fraction of MWCNTs, as well as the uniform dispersion of MWCNTs in the bentonite clays. In comparison to the 8% MWCNTs/bentonite ceramic composites, the electrical conductivity of heptane-MWCNTs/Gobu bentonite ( $\sigma = 397 \text{ S.m}^{-1}$ ) and heptane-MWCNTs/Atyali ( $\sigma = 305 \text{ S.m}^{-1}$ ) composites was 2–5 times higher than the conductivity of composites obtained with cyclohexane CNTs-cyclohexane-MWCNT/Atyali ( $\sigma = 78 \text{ S.m}^{-1}$ ) and cyclohexane-multi-walled carbon nanotube/Gobu ( $\sigma = 111.5 \text{ S.m}^{-1}$ ) depending on the structure, diameter distribution, purity, the number of layers, and the type and amount of defects in the inner and outer layers of Hep-MWCNTs, causing better dispersion in bentonite clays. Thus, in conclusion, one can say that the composite matrix of

Azerbaijani natural bentonite and MWCNTs, after displaying excellent thermal stability and high conductivity, could be employed for various applications such as electrodes and thermocouples.

## 5. Conclusions and Prospective Outlook

In summary, the advances in CNT growth based on structure, growth mechanism, mass production, purification methods from several natural materials, and their potential applications throughout the last two decades were reviewed. Natural materials such as garnet, siliceous breccia, natural laterite, natural lava, nontronite, chrysotile, bentonite, and many more proved to be suitable catalysts for carbon nanomaterial growth, which, after appropriate wet chemical treatment, can result in SWCNTs/MWCNTs. The list provided in Table 1 exhibits a promising and interesting perspective of these cheaper resources for carbon nanomaterials synthesis. From the reviewed studies, it is found that natural materials, which have even less than 0.1 wt. of the percentage amount of the metal oxide trace, could promote the growth of CNTs of good quality. These results encourage us to explore the benefits of such natural resources with the lowest costs and less impact on the environment. The TGA results of such CNTs show an oxidation peak nearby 600 °C, confirming the thermal and oxidation stability of CNTs.

**Table 1.** Natural materials used as a catalyst source for the synthesis of carbon nanomaterials.

Natural Material	Origin	Carbon Source	Process	Temperature (°C)	Type of Carbon Nanomaterial	Ref.
Garnet	Japan	City Gas	CVD	1000	MWCNT	[60]
Lava	Italy	Ethylene	CVD	700	CNF	[74]
Bentonite	Germany	Ethylene	CVD	650	MWCNT	[66]
Forsterite	USA	Methane	CVD	800–900	Amorphous carbon	[61]
Diopside	Pakistan	Methane	CVD	800–900	Amorphous carbon	[61]
Quartz	Japan	Methane	CVD	800–900	Amorphous carbon	[61]
Magnesite	Brazil	Methane	CVD	800–900	SWCNT, MWCNT	[61]
Brucite	USA	Methane	CVD	800–900	SWCNT, MWCNT	[61]
Bentonite	Greece	Acetylene	CVD	700	CNF	[63]
Sepiolite	China	Methane	CVD	9000	CNT	[79]
Natural Laterite	New Caledonia	Ethylene	CVD	700–900	CNT, CNS	[68]
Siliceous Breccia	New Caledonia	Ethylene	CVD	700	CNT	[71]
Vermiculite	China	Ethylene, Propylene, Liquefied Petroleum Gas	CVD	600–800	MWCNT	[72]
Chrysotile	Brazil	Ethanol	CVD	600–900	CNT, CNF, amorphous carbon	[62]
Blended Iron Formation	India	Benzylamine	AACCVD	-	N-MWCNT	[77]
Wollastonite	China	Ethylene	CVD	700	CNT	[78]
Nontronite	USA	Methane	HFCVD		CNT	[81]
Sepiolite	China	Methane	CVD	900	SWCNT	[81]

Another important benefit of using such natural minerals as catalyst sources for CNTs synthesis is that no additional pre-treatment of the catalyst is required. This suggests that such common natural materials have a strong potential to replace the existing expensive

catalysts and restricted potential applications on a large scale. Employing natural minerals or mineral oxides could help us to reduce the high processing cost. Without a doubt, the published scientific research results are very encouraging for the CNTs industry, but a study that is more detailed needs to be performed to understand carbon nanomaterials' growth using natural materials. Further, the as-obtained CNTs were found to have a wide distribution of their diameters as well as being strongly entangled with the impurity of the catalyst particle. However, natural materials always possess a complex elemental and structural composition, and few elements (such as K and P) are detrimental to CNTs high-yield production. On the other hand, materials such as chrysotile, despite showing excellent applications in the commercial and industrial sectors, are considered hazardous and cause diseases such as lung fibrous, mesothelioma, and lung cancer upon exposure [94]. Therefore, such materials should be avoided for the synthesis of carbon nanomaterials. Further, these natural materials have a minor content of natural metals or metal oxide traces resulting from natural geological processes and weathering conditions, and during the CVD growth process, it could be difficult to modify them under the optimal condition. This also causes difficulty in fully understanding the growth mechanism.

For these issues, only a few studies have been carried out in detail. Therefore, additional scientific work is needed to be conducted in terms of chirality and purification to scope the suitable technology level for commercial application and a sustainable society.

**Funding:** This research received no external funding.

**Institutional Review Board Statement:** Not applicable.

**Informed Consent Statement:** Not applicable.

**Data Availability Statement:** No new data were created or analyzed in this study.

**Conflicts of Interest:** The authors declare no conflict of interest.

## References

1. Reibold, M.; Paufler, P.; Levin, A.A.; Kochmann, W.; Pätzke, N.; Meyer, D.C. Materials: Carbon nanotubes in an ancient Damascus sabre. *Nature* **2006**, *444*. [[CrossRef](#)] [[PubMed](#)]
2. Kokarneswaran, M.; Selvaraj, P.; Ashokan, T.; Perumal, S.; Sellappan, P.; Murugan, K.D.; Ramalingam, S.; Mohan, N.; Chandrasekaran, V. Discovery of Carbon nanotubes in 6th Century BC potteries from Keeladi, India. *Sci. Rep.* **2020**, *10*, 339–343. [[CrossRef](#)] [[PubMed](#)]
3. Iijima, S. Helical microtubules of graphitic carbon. *Nature* **1991**. [[CrossRef](#)]
4. Che, J.; Çağın, T.; Goddard, W.A. Thermal conductivity of carbon nanotubes. *Nanotechnology* **2000**, *11*, 65. [[CrossRef](#)]
5. Hone, J.; Llaguno, M.C.; Biercuk, M.J.; Johnson, A.T.; Batlogg, B.; Benes, Z.; Fischer, J.E. Thermal properties of carbon nanotubes and nanotube-based materials. *Appl. Phys. A Mater. Sci. Process.* **2002**, *74*, 339–343. [[CrossRef](#)]
6. Han, Z.; Fina, A. Thermal conductivity of carbon nanotubes and their polymer nanocomposites: A review. *Prog. Polym. Sci.* **2011**, *36*, 914–944. [[CrossRef](#)]
7. Kumanek, B.; Janas, D. Thermal conductivity of carbon nanotube networks: A review. *J. Mater. Sci.* **2019**, *54*, 7397–7427. [[CrossRef](#)]
8. Nejad, S.M.; Srivastava, R.; Bellussi, F.M.; Thielemann, H.C.; Asinari, P.; Fasano, M. Nanoscale thermal properties of carbon nanotubes/epoxy composites by atomistic simulations. *Int. J. Therm. Sci.* **2021**, *159*, 106588. [[CrossRef](#)]
9. Fischer, J.E.; Johnson, A.T. Electronic properties of carbon nanotubes. *Curr. Opin. Solid State Mater. Sci.* **1999**, *4*, 28–33. [[CrossRef](#)]
10. Janas, D.; Milowska, K.Z.; Bristowe, P.D.; Koziol, K.K.K. Improving the electrical properties of carbon nanotubes with interhalogen compounds. *Nanoscale* **2017**, *9*, 3212–3222. [[CrossRef](#)]
11. Barnett, C.J.; Gowenlock, C.E.; Welsby, K.; White, A.O.; Barron, A.R. Spatial and Contamination-Dependent Electrical Properties of Carbon Nanotubes. *Nano Lett.* **2018**, *18*, 695–700. [[CrossRef](#)] [[PubMed](#)]
12. Mathur, R.B.; Pande, S.; Singh, B.P.; Dhami, T.L. Electrical and mechanical properties of multi-walled carbon nanotubes reinforced PMMA and PS composites. *Polym. Compos.* **2008**, *29*, 717–727. [[CrossRef](#)]
13. Salvat, J.P.; Bonard, J.M.; Thomson, N.B.; Kulik, A.J.; Forró, L.; Benoit, W.; Zuppiroli, L. Mechanical properties of carbon nanotubes. *Appl. Phys. A Mater. Sci. Process.* **1999**, *69*, 255–260. [[CrossRef](#)]
14. Ruoff, R.S.; Qian, D.; Liu, W.K. Mechanical properties of carbon nanotubes: Theoretical predictions and experimental measurements. *C. R. Phys.* **2003**, *4*, 993–1008. [[CrossRef](#)]
15. Coleman, J.N.; Khan, U.; Blau, W.J.; Gun'ko, Y.K. Small but strong: A review of the mechanical properties of carbon nanotube-polymer composites. *Carbon* **2006**, *44*, 1624–1652. [[CrossRef](#)]

16. Lei, X.; Natsuki, T.; Shi, J.; Ni, Q.Q. Analysis of carbon nanotubes on the mechanical properties at atomic scale. *J. Nanomater.* **2011**, *2011*, 805313. [[CrossRef](#)]
17. Tans, S.J.; Devoret, M.H.; Dai, H.; Thess, A.; Smalley, R.E.; Geerligs, L.J.; Dekker, C. Individual single-wall carbon nanotubes as quantum wires. *Nature* **1997**, *386*, 474–477. [[CrossRef](#)]
18. Sinitsyn, N.I.; Gulyaev, Y.V.; Torgashov, G.V.; Chernozatonskii, L.A.; Kosakovskaya, Z.Y.; Zakharchenko, Y.F.; Kiselev, N.A.; Musatov, A.L.; Zhbanov, A.I.; Mevlyut, S.T.; et al. Thin films consisting of carbon nanotubes as a new material for emission electronics. *Appl. Surf. Sci.* **1997**, *111*, 145–150. [[CrossRef](#)]
19. Tans, S.J.; Verschueren, A.R.M.; Dekker, C. Room-temperature transistor based on a single carbon nanotube. *Nature* **1998**, *393*, 49–52. [[CrossRef](#)]
20. Sharma, P.; Ahuja, P. Recent advances in carbon nanotube-based electronics. *Mater. Res. Bull.* **2008**, *43*, 2517–2526. [[CrossRef](#)]
21. Peng, L.M.; Zhang, Z.; Wang, S. Carbon nanotube electronics: Recent advances. *Mater. Today* **2014**, *17*, 433–442. [[CrossRef](#)]
22. Si, J.; Xu, L.; Zhu, M.; Zhang, Z.; Peng, L.M. Advances in High-Performance Carbon-Nanotube Thin-Film Electronics. *Adv. Electron. Mater.* **2019**, *5*, 1900122. [[CrossRef](#)]
23. Xiong, C.; Li, M.; Zhao, W.; Duan, C.; Ni, Y. Flexible N-Doped reduced graphene oxide/carbon Nanotube-MnO<sub>2</sub> film as a Multifunctional Material for High-Performance supercapacitors, catalysts and sensors. *J. Mater.* **2020**, *6*, 523–531. [[CrossRef](#)]
24. Xiong, C.; Lin, X.; Liu, H.; Li, M.; Li, B.; Jiao, S.; Zhao, W.; Duan, C.; Dai, L.; Ni, Y. Fabrication of 3D Expanded Graphite-Based (MnO<sub>2</sub> Nanowalls and PANI Nanofibers) Hybrid as Bifunctional Material for High-Performance Supercapacitor and Sensor. *J. Electrochem. Soc.* **2019**, *166*, A3965–A3971. [[CrossRef](#)]
25. Zaporotskova, I.V.; Boroznina, N.P.; Parkhomenko, Y.N.; Kozhitov, L.V. Carbon nanotubes: Sensor properties. A review. *Mod. Electron. Mater.* **2016**, *2*, 95–105. [[CrossRef](#)]
26. Schroeder, V.; Savagatrup, S.; He, M.; Lin, S.; Swager, T.M. Carbon nanotube chemical sensors. *Chem. Rev.* **2019**, *119*, 599–663. [[CrossRef](#)]
27. Hwang, S.I.; Star, A. Picking Flowers with Carbon Nanotube Sensors. *ACS Cent. Sci.* **2020**, *6*, 461–463. [[CrossRef](#)]
28. Xiong, C.; Li, M.; Zhao, W.; Duan, C.; Dai, L.; Shen, M.; Xu, Y.; Ni, Y. A smart paper@polyaniline nanofibers incorporated vitrimer bifunctional device with reshaping, shape-memory and self-healing properties applied in high-performance supercapacitors and sensors. *Chem. Eng. J.* **2020**, *396*, 125318. [[CrossRef](#)]
29. Bianco, A.; Kostarelos, K.; Prato, M. Applications of carbon nanotubes in drug delivery. *Curr. Opin. Chem. Biol.* **2005**, *9*, 674–679. [[CrossRef](#)]
30. Bhirde, A.A.; Patel, V.; Gavard, J.; Zhang, G.; Sousa, A.A.; Masedunskas, A.; Leapman, R.D.; Weigert, R.; Gutkind, J.S.; Rusling, J.F. Targeted killing of cancer cells in vivo and in vitro with EGF-directed carbon nanotube-based drug delivery. *ACS Nano* **2009**, *3*, 307–316. [[CrossRef](#)]
31. Tangboriboon, N. Carbon and Carbon Nanotube Drug Delivery and Its Characterization, Properties, and Applications. In *Nanocarriers for Drug Delivery*; Elsevier: Amsterdam, The Netherlands, 2019; pp. 451–467.
32. Cheng, H.M.; Yang, Q.H.; Liu, C. Hydrogen storage in carbon nanotubes. *Carbon* **2001**, *39*, 1447–1454. [[CrossRef](#)]
33. Doğan, E.E.; Tokcan, P.; Kizilduman, B.K. Storage of Hydrogen in Activated Carbons and Carbon Nanotubes. *Adv. Mater. Sci.* **2019**, *18*, 5–16. [[CrossRef](#)]
34. Tripathi, P.; Bhatnagar, A.; Ramesh, A.; Vishwakarma, A.K.; Singh, S.; Bailmare, D.B.; Deshmukh, A.D.; Gupta, B.K.; Srivastava, O.N. Radially aligned CNTs derived carbon hollow cylinder architecture for efficient energy storage. *Electrochim. Acta* **2020**, *354*, 136650. [[CrossRef](#)]
35. Xia, X.; Zhang, Y.; Fan, Z.; Chao, D.; Xiong, Q.; Tu, J.; Zhang, H.; Fan, H.J. Novel Metal@CARBON spheres core-shell arrays by controlled self-assembly of carbon nanospheres: A stable and flexible supercapacitor electrode. *Adv. Energy Mater.* **2015**, *5*. [[CrossRef](#)]
36. Sun, L.; Wang, X.; Wang, Y.; Zhang, Q. Roles of carbon nanotubes in novel energy storage devices. *Carbon* **2017**, *122*, 462–474. [[CrossRef](#)]
37. Yu, D.; Goh, K.; Wang, H.; Wei, L.; Jiang, W.; Zhang, Q.; Dai, L.; Chen, Y. Scalable synthesis of hierarchically structured carbon nanotube-graphene fibres for capacitive energy storage. *Nat. Nanotechnol.* **2014**, *9*, 555–562. [[CrossRef](#)]
38. Lu, Z.; Raad, R.; Safaei, F.; Xi, J.; Liu, Z.; Foroughi, J. Carbon nanotube based fiber supercapacitor as wearable energy storage. *Front. Mater.* **2019**, *6*, 138. [[CrossRef](#)]
39. Xiong, C.; Li, B.; Liu, H.; Zhao, W.; Duan, C.; Wu, H.; Ni, Y. A smart porous wood-supported flower-like NiS/Ni conjunction with vitrimer co-effect as a multifunctional material with reshaping, shape-memory, and self-healing properties for applications in high-performance supercapacitors, catalysts, and sensors. *J. Mater. Chem. A* **2020**, *8*, 10898–10908. [[CrossRef](#)]
40. Xiong, C.; Li, M.; Nie, S.; Dang, W.; Zhao, W.; Dai, L.; Ni, Y. Non-carbonized porous lignin-free wood as an effective scaffold to fabricate lignin-free Wood@Polyaniline supercapacitor material for renewable energy storage application. *J. Power Sources* **2020**, *471*, 228448. [[CrossRef](#)]
41. Castillejos, E.; Serp, P. Carbon Nanotubes for Catalytic Applications. In *Carbon Nanotubes and Related Structures*; Wiley-VCH Verlag GmbH & Co. KGaA: Weinheim, Germany, 2010; pp. 321–347.
42. Esteves, L.M.; Oliveira, H.A.; Passos, F.B. Carbon nanotubes as catalyst support in chemical vapor deposition reaction: A review. *J. Ind. Eng. Chem.* **2018**, *65*, 1–12. [[CrossRef](#)]
43. Harrison, B.S.; Atala, A. Carbon nanotube applications for tissue engineering. *Biomaterials* **2007**, *28*, 344–353. [[CrossRef](#)] [[PubMed](#)]

44. Baughman, R.H.; Zakhidov, A.A.; De Heer, W.A. Carbon nanotubes—The route toward applications. *Science* **2002**, *297*, 787–792. [[CrossRef](#)] [[PubMed](#)]
45. Kaushik, B.K.; Majumder, M.K. Carbon nanotube: Properties and applications. In *Carbon Nanotube Based VLSI Interconnects*; Springer: New Delhi, India, 2015; pp. 17–37. [[CrossRef](#)]
46. Zhai, P.; Isaacs, J.A.; Eckelman, M.J. Net energy benefits of carbon nanotube applications. *Appl. Energy* **2016**, *173*, 624–634. [[CrossRef](#)]
47. Venkataraman, A.; Amadi, E.V.; Chen, Y.; Papadopoulos, C. Carbon Nanotube Assembly and Integration for Applications. *Nanoscale Res. Lett.* **2019**, *14*, 1–47. [[CrossRef](#)]
48. Zhang, Q.; Huang, J.Q.; Zhao, M.Q.; Qian, W.Z.; Wei, F. Carbon nanotube mass production: Principles and processes. *ChemSusChem* **2011**, *4*, 864–889. [[CrossRef](#)]
49. Kumar, M.; Ando, Y. Chemical vapor deposition of carbon nanotubes: A review on growth mechanism and mass production. *J. Nanosci. Nanotechnol.* **2010**, *10*, 3739–3758. [[CrossRef](#)]
50. Ghaemi, F.; Ali, M.; Yunus, R.; Othman, R.N. Synthesis of carbon nanomaterials using catalytic chemical vapor deposition technique. In *Synthesis, Technology and Applications of Carbon Nanomaterials*; Elsevier: Amsterdam, The Netherlands, 2018; pp. 1–27. ISBN 9780128157572.
51. See, C.H.; Harris, A.T. A review of carbon nanotube synthesis via fluidized-bed chemical vapor deposition. *Ind. Eng. Chem. Res.* **2007**, *46*, 997–1012. [[CrossRef](#)]
52. Danafar, F.; Fakhru'l-Razi, A.; Salleh, M.A.M.; Biak, D.R.A. Fluidized bed catalytic chemical vapor deposition synthesis of carbon nanotubes—A review. *Chem. Eng. J.* **2009**, *155*, 37–48. [[CrossRef](#)]
53. Ayre, G.N.; Uchino, T.; Mazumder, B.; Hector, A.L.; Hutchison, J.L.; Smith, D.C.; Ashburn, P.; De Groot, C.H. On the mechanism of carbon nanotube formation: The role of the catalyst. *J. Phys. Condens. Matter* **2011**, *23*, 394201. [[CrossRef](#)]
54. Gao, J.; Zhong, J.; Bai, L.; Liu, J.; Zhao, G.; Sun, X. Revealing the role of catalysts in carbon nanotubes and nanofibers by scanning transmission X-Ray microscopy. *Sci. Rep.* **2014**, *4*, 1–6. [[CrossRef](#)] [[PubMed](#)]
55. Li, M.; Liu, X.; Zhao, X.; Yang, F.; Wang, X.; Li, Y. Metallic Catalysts for Structure-Controlled Growth of Single-Walled Carbon Nanotubes. *Top. Curr. Chem.* **2017**, *375*, 1–43. [[CrossRef](#)]
56. Yahyazadeh, A.; Khoshandam, B. Carbon nanotube synthesis via the catalytic chemical vapor deposition of methane in the presence of iron, molybdenum, and iron–molybdenum alloy thin layer catalysts. *Results Phys.* **2017**, *7*, 3826–3837. [[CrossRef](#)]
57. Homma, Y.; Kobayashi, Y.; Ogino, T.; Takagi, D.; Ito, R.; Jung, Y.J.; Ajayan, P.M. Role of transition metal catalysts in single-walled carbon nanotube growth in chemical vapor deposition. *J. Phys. Chem. B* **2003**, *107*, 12161–12164. [[CrossRef](#)]
58. Ur Rashid, H.; Yu, K.; Naveed Umar, M.; Naveed Anjum, M.; Khan, K.; Ahmad, N.; Tariq Jan, M. Catalyst role in chemical vapor deposition (CVD) process: A review. *Rev. Adv. Mater. Sci.* **2015**, *40*, 235–248.
59. Hoecker, C.; Smail, F.; Pick, M.; Boies, A. The influence of carbon source and catalyst nanoparticles on CVD synthesis of CNT aerogel. *Chem. Eng. J.* **2017**, *314*, 388–395. [[CrossRef](#)]
60. Endo, M.; Takeuchi, K.; Kim, Y.A.; Park, K.C.; Ichiki, T.; Hayashi, T.; Fukuyo, T.; Iinou, S.; Su, D.S.; Terrones, M.; et al. Simple synthesis of multiwalled carbon nanotubes from natural resources. *ChemSusChem* **2008**, *1*, 820–822. [[CrossRef](#)]
61. Kawasaki, S.; Shinoda, M.; Shimada, T.; Okino, F.; Touhara, H. Single-walled carbon nanotubes grown on natural minerals. *Carbon* **2006**, *44*, 2139–2141. [[CrossRef](#)]
62. Lemos, B.R.S.; Soares, A.R.; Teixeira, A.P.C.; Ardisson, J.D.; Fernandez-Outon, L.E.; Amorim, C.C.; Lago, R.M.; Moura, F.C.C. Growth of carbon structures on chrysotile surface for organic contaminants removal from wastewater. *Chemosphere* **2016**, *159*, 602–609. [[CrossRef](#)]
63. Bakandritsos, A.; Simopoulos, A.; Petridis, D. Iron changes in natural and Fe(III) loaded montmorillonite during carbon nanotube growth. *Nanotechnology* **2006**, *17*, 1112–1117. [[CrossRef](#)]
64. Kadleciková, M.; Breza, J.; Jesenák, K.; Pastorková, K.; Luptáková, V.; Kolmačka, M.; Vojačková, A.; Michalka, M.; Vávra, I.; Križanová, Z. The growth of carbon nanotubes on montmorillonite and zeolite (clinoptilolite). *Appl. Surf. Sci.* **2008**, *254*, 5073–5079. [[CrossRef](#)]
65. Zhang, W.D.; Phang, I.Y.; Liu, T. Growth of carbon nanotubes on clay: Unique nanostructured filler for high-performance polymer nanocomposites. *Adv. Mater.* **2006**, *18*, 73–77. [[CrossRef](#)]
66. Rinaldi, A.; Zhang, J.; Mizera, J.; Girgsdies, F.; Wang, N.; Hamid, S.B.A.; Schlögl, R.; Su, D.S. Facile synthesis of carbon nanotube/natural bentonite composites as a stable catalyst for styrene synthesis. *Chem. Commun.* **2008**, 6528–6530. [[CrossRef](#)]
67. Huseynov, A.; Israfilov, A.; Mammadova, S.; Abdullayeva, S.; Sokolov, S.; Goryunkov, A.; Guliyev, A. Fabrication and characterization of MWCNT/natural Azerbaijani bentonite electroconductive ceramic composites. *J. Compos. Mater.* **2019**, *53*, 3909–3923. [[CrossRef](#)]
68. Kumar, A.; Kostikov, Y.; Orberger, B.; Nessim, G.D.; Mariotto, G. Natural Laterite as a Catalyst Source for the Growth of Carbon Nanotubes and Nanospheres. *ACS Appl. Nano Mater.* **2018**, *1*, 6046–6054. [[CrossRef](#)]
69. Secchi, M.; Zanatta, M.; Borovin, E.; Bortolotti, M.; Kumar, A.; Giarola, M.; Sanson, A.; Orberger, B.; Daldosso, N.; Gialanella, S.; et al. Mineralogical investigations using XRD, XRF, and Raman spectroscopy in a combined approach. *J. Raman Spectrosc.* **2018**, *49*, 1023–1030. [[CrossRef](#)]

70. Duée, C.; Maubec, N.; Laperche, V.; Capar, L.; Bourguignon, A.; Bourrat, X.; Mendili, Y.E.; Chateigner, D.; Gascoin, S.; Mariotto, G.; et al. Combined mineralogy and chemistry on drill cores: Challenging for on-line-real-time analyses. In Proceedings of the 14th Biennial SGA Meeting, Québec, QC, Canada, 20–23 August 2017; Volume 3, pp. 1241–1244.
71. Kumar, A.; Kostikov, Y.; Zanatta, M.; Sorarù, G.D.; Orberger, B.; Nessim, G.D.; Mariotto, G. Carbon nanotubes synthesis using siliceous breccia as a catalyst source. *Diam. Relat. Mater.* **2019**, *97*, 107433. [[CrossRef](#)]
72. Zhang, Q.; Zhao, M.Q.; Huang, J.Q.; Liu, Y.; Wang, Y.; Qian, W.Z.; Wei, F. Vertically aligned carbon nanotube arrays grown on a lamellar catalyst by fluidized bed catalytic chemical vapor deposition. *Carbon* **2009**, *47*, 2600–2610. [[CrossRef](#)]
73. Wei, F.; Zhang, Q.; Qian, W.Z.; Yu, H.; Wang, Y.; Luo, G.H.; Xu, G.H.; Wang, D.Z. The mass production of carbon nanotubes using a nano-agglomerate fluidized bed reactor: A multiscale space-time analysis. *Powder Technol.* **2008**, *183*, 10–20. [[CrossRef](#)]
74. Dang, S.S.; Chen, X.W. Natural lavas as catalysts for efficient production of carbon nanotubes and nanofibers. *Angew. Chemie Int. Ed.* **2007**, *46*, 1823–1824. [[CrossRef](#)]
75. Su, D.S.; Rinaldi, A.; Frandsen, W.; Weinberg, G. Nanocarbons: Efficient synthesis using natural lava as supported catalyst. *Phys. Status Solidi* **2007**, *244*, 3916–3919. [[CrossRef](#)]
76. Katsuta, N.; Shimizu, I.; Helmstaedt, H.; Takano, M.; Kawakami, S.; Kumazawa, M. Major element distribution in Archean banded iron formation (BIF): Influence of metamorphic differentiation. *J. Metamorph. Geol.* **2012**, *30*, 457–472. [[CrossRef](#)]
77. Jimenez-Ramirez, L.E.; Kashina, S.; Galindo, R.; Fuentes-Ramirez, R.; Verma, S.K.; Fajardo-Diaz, J.L.; López-Urías, F.; Muñoz-Sandoval, E. Synthesis, morphology, magnetic and electrochemical studies of nitrogen-doped multiwall carbon nanotubes fabricated using banded iron-formation as catalyst. *J. Alloy. Compd.* **2020**, *835*, 155200. [[CrossRef](#)]
78. Zhao, M.Q.; Zhang, Q.; Huang, J.Q.; Nie, J.Q.; Wei, F. Advanced materials from natural materials: Synthesis of aligned carbon nanotubes on wollastonites. *ChemSusChem* **2010**, *3*, 453–459. [[CrossRef](#)] [[PubMed](#)]
79. Nie, J.Q.; Zhang, Q.; Zhao, M.Q.; Huang, J.Q.; Wen, Q.; Cui, Y.; Qian, W.Z.; Wei, F. Synthesis of high quality single-walled carbon nanotubes on natural sepiolite and their use for phenol absorption. *Carbon* **2011**, *49*, 1568–1580. [[CrossRef](#)]
80. Dresselhaus, M.S.; Dresselhaus, G.; Saito, R.; Jorio, A. Raman spectroscopy of carbon nanotubes. *Phys. Rep.* **2005**, *409*, 47–99. [[CrossRef](#)]
81. Pastorková, K.; Jesenák, K.; Kadlecíková, M.; Breza, J.; Kolmačka, M.; Čaplovicová, M.; Lazišťan, F.; Michalka, M. The growth of multi-walled carbon nanotubes on natural clay minerals (kaolinite, nontronite and sepiolite). *Appl. Surf. Sci.* **2012**, *258*, 2661–2666. [[CrossRef](#)]
82. Behmel, S.; Damour, M.; Ludwig, R.; Rodriguez, M.J. Water quality monitoring strategies—A review and future perspectives. *Sci. Total Environ.* **2016**, *571*, 1312–1329. [[CrossRef](#)]
83. Salari, M.; Dehghani, M.H.; Azari, A.; Motevalli, M.D.; Shabanloo, A.; Ali, I. High performance removal of phenol from aqueous solution by magnetic chitosan based on response surface methodology and genetic algorithm. *J. Mol. Liq.* **2019**, *285*, 146–157. [[CrossRef](#)]
84. Du, W.; Sun, J.; Zan, Y.; Zhang, Z.; Ji, J.; Dou, M.; Wang, F. Biomass-derived nitrogen-doped hierarchically porous carbon networks as efficient absorbents for phenol removal from wastewater over a wide pH range. *RSC Adv.* **2017**, *7*, 46629–46635. [[CrossRef](#)]
85. Fu, Y.; Shen, Y.; Zhang, Z.; Ge, X.; Chen, M. Activated biochars derived from rice husk via one- and two-step KOH-catalyzed pyrolysis for phenol adsorption. *Sci. Total Environ.* **2019**, *646*, 1567–1577. [[CrossRef](#)] [[PubMed](#)]
86. Ethaib, S.; Erabee, I.K. Abdulsahib 2018 Removal of Methylene Blue Dye from Synthetic Wastewater using Kenaf Core and Activated Carbon. *Int. J. Eng. Technol.* **2018**, *7*, 909. [[CrossRef](#)]
87. Arumugam, N.; Chelliapan, S.; Kamyab, H.; Thirugnana, S.; Othman, N.; Nasri, N. Treatment of Wastewater Using Seaweed: A Review. *Int. J. Environ. Res. Public Health* **2018**, *15*, 2851. [[CrossRef](#)]
88. Bao, Y.; Zhang, G. Study of adsorption characteristics of methylene blue onto activated carbon made by salix psammophila. In Proceedings of the Energy Procedia; Elsevier Ltd.: Amsterdam, The Netherlands, 2012; Volume 16, pp. 1141–1146.
89. Pathania, D.; Sharma, S.; Singh, P. Removal of methylene blue by adsorption onto activated carbon developed from Ficus carica bast. *Arab. J. Chem.* **2017**, *10*, S1445–S1451. [[CrossRef](#)]
90. Ahmad, I.; Yazdani, B.; Zhu, Y. Recent Advances on Carbon Nanotubes and Graphene Reinforced Ceramics Nanocomposites. *Nanomaterials* **2015**, *5*, 90–114. [[CrossRef](#)]
91. Sorarù, G.D.; Kacha, G.; Campostrini, R.; Ponzoni, A.; Donarelli, M.; Kumar, A.; Mariotto, G. The effect of B-doping on the electrical conductivity of polymer-derived Si(B)OC ceramics. *J. Am. Ceram. Soc.* **2017**, *100*, 4611–4621. [[CrossRef](#)]
92. Delbari, S.A.; Nayebi, B.; Ghasali, E.; Shokouhimehr, M.; Shahedi Asl, M. Spark plasma sintering of TiN ceramics codoped with SiC and CNT. *Ceram. Int.* **2019**, *45*, 3207–3216. [[CrossRef](#)]
93. Popov, O.; Vleugels, J.; Huseynov, A.; Vishnyakov, V. Reactive sintering of TiB<sub>2</sub>-SiC-CNT ceramics. *Ceram. Int.* **2019**, *45*, 22769–22774. [[CrossRef](#)]
94. Bernstein, D.; Dunnigan, J.; Hesterberg, T.; Brown, R.; Antonio, J.; Velasco, L.; Barrera, R.; Hoskins, J.; Gibbs, A. Health risk of chrysotile revisited. *Crit. Rev. Toxicol.* **2013**, *43*, 154–183. [[CrossRef](#)]